

**High-quality ultrastructural preservation using cryofixation for 3D electron microscopy of  
genetically labeled tissues**

Tin Ki Tsang<sup>1\*</sup>, Eric A. Bushong<sup>2\*</sup>, Daniela Boassa<sup>2</sup>, Junru Hu<sup>2</sup>, Benedetto Romoli<sup>3</sup>, Sebastien  
Phan<sup>2</sup>, Davide Dulcis<sup>3</sup>, Chih-Ying Su<sup>1δ</sup> and Mark H. Ellisman<sup>2,4δ</sup>

<sup>1</sup>Neurobiology Section, Division of Biological Sciences,  
University of California, San Diego, La Jolla, CA 92093, USA

<sup>2</sup>National Center for Microscopy and Imaging Research, Center for Research in Biological  
Systems, University of California, San Diego, La Jolla, CA 92093, USA

<sup>3</sup>Department of Psychiatry, School of Medicine, University of California, San Diego, La Jolla, CA  
92093, USA

<sup>4</sup>Department of Neurosciences, School of Medicine  
University of California, San Diego, La Jolla, CA 92093, USA

\* These authors contributed equally to this work.

δCorrespondence: [mellisman@ucsd.edu](mailto:mellisman@ucsd.edu) (M.H.E); [c8su@ucsd.edu](mailto:c8su@ucsd.edu) (C.Y.S)

## ABSTRACT

Electron microscopy (EM) offers unparalleled power to study cell substructures at the nanoscale. Cryofixation by high-pressure freezing offers optimal morphological preservation, as it captures cellular structures instantaneously in their near-native states. However, the applicability of cryofixation is limited by its incompatibilities with diaminobenzidine labeling using genetic EM tags and the high-contrast *en bloc* staining required for serial block-face scanning electron microscopy (SBEM). In addition, it is challenging to perform correlated light and electron microscopy (CLEM) with cryofixed samples. Consequently, these powerful methods cannot be applied to address questions requiring optimal morphological preservation. Here we developed an approach that overcomes these limitations; it enables genetically labeled, cryofixed samples to be characterized with SBEM and 3D CLEM. Our approach is broadly applicable, as demonstrated in cultured cells, *Drosophila* olfactory organ and mouse brain. This optimization exploits the potential of cryofixation, allowing quality ultrastructural preservation for diverse EM applications.



## INTRODUCTION

The answers to many questions in biology lie in the ability to examine the relevant biological structures accurately at high resolution. Electron microscopy (EM) offers the unparalleled power to study cellular morphology and structure at nanoscale resolution (Leapman, 2004). Cryofixation by high-pressure freezing (hereafter referred to as cryofixation) is the optimal fixation method for samples of thicknesses up to approximately 500  $\mu\text{m}$  (Dahl and Staehelin, 1989; McDonald, 1999; Moor, 1987; Shimoni et al., 1998). By rapidly freezing the samples in liquid nitrogen ( $-196\text{ }^{\circ}\text{C}$ ) under high pressure ( $\sim 2100\text{ bar}$ ), cryofixation immobilizes cellular structures within milliseconds and preserves them in their near-native states. In contrast, cross-linking based chemical fixation takes place at higher temperatures ( $\geq 4\text{ }^{\circ}\text{C}$ ) and depends on the infiltration of aldehyde fixatives, a process which takes seconds to minutes to complete. During chemical fixation, cellular structures may deteriorate or undergo rearrangement (Korogod et al., 2015; Steinbrecht and Müller, 1987; Szczesny et al., 1996) and enzymatic reactions can proceed (Kellenberger et al., 1992; Sabatini, 1963), potentially resulting in significant morphological artefacts.

Cryofixation is especially critical, and often necessary, for properly fixing tissues with cell walls or cuticles that are impermeable to chemical fixatives, such as samples from yeast, plant, *C. elegans*, and *Drosophila* (Ding, 1993; Doroquez et al., 2014; Kaeser et al., 1989; Kiss et al., 1990; McDonald, 2007; Müller-Reichert et al., 2003; Shanbhag et al., 1999, 2000; Winey et al., 1995). As cryofixation instantaneously halts all cellular processes, it also provides the temporal control needed to capture fleeting biological events in a dynamic process (Hess et al., 2000; Watanabe et al., 2013; Watanabe et al., 2013; Watanabe et al., 2014).

Despite the clear benefits of cryofixation, it is incompatible with diaminobenzidine (DAB) labeling reactions by genetic EM tags. For example, APEX2 (enhanced ascorbate peroxidase) is an engineered peroxidase that catalyzes DAB reaction to render target structures electron

dense (Lam et al., 2015; Martell et al., 2012). Despite the successful applications of APEX2 to three-dimensional (3D) EM (Joesch et al., 2016), there has been no demonstration that APEX2 or other genetic EM tags can be activated following cryofixation. Conventionally, cryofixation is followed by freeze-substitution (Steinbrecht and Müller, 1987), during which water in the sample is replaced by organic solvents. However, the resulting dehydrated environment is incompatible with the aqueous enzymatic reactions required for DAB labeling by genetic EM tags.

EM structures can also be genetically labeled with fluorescent markers through correlated light and electron microscopy (CLEM). Yet, performing CLEM with cryofixed samples also presents challenges. Fluorescence microscopy commonly takes place either before cryofixation (Brown et al., 2009; Kolotuev et al., 2010; McDonald, 2009) or at a later stage after the sample is embedded (Kukulski et al., 2011; Nixon et al., 2009; Schwarz and Humbel, 2009). However, if the specimen is dissected from live animals, the time taken to acquire fluorescence images delays cryofixation and could cause ultrastructural deterioration. In order for fluorescence microscopy to take place after embedding, special acrylic resins need to be used (Kukulski et al., 2011; Nixon et al., 2009; Schwarz and Humbel, 2009) and only a low concentration of osmium tetroxide stain can be tolerated (De Boer et al., 2015; Watanabe et al., 2011). Although one can in principle perform fluorescence microscopy in cryofixed samples after rehydration, fluorescence images have only been acquired in sucrose-infiltrated cryosections (300-500 nm) (Ripper et al., 2008; Stierhof and El Kasmi, 2010). Moreover, no protocol has been developed to prepare large cryofixed tissues expressing genetic CLEM markers for high-contrast EM imaging. These constraints limit the applicability of CLEM for cryofixed samples.

Another disadvantage of cryofixation is that *en bloc* staining during freeze-substitution is often inadequate. As a result, post-staining of ultramicrotomy sections is frequently needed for cryofixed samples (Shanbhag et al., 1999, 2000; Takemura et al., 2013). However, post-staining could be labor-intensive and time-consuming, especially for volume EM (Ryan et al., 2016;

Zheng et al., 2017). Critically, on-section staining is impossible for samples imaged with block-face volume EM techniques (Briggman and Bock, 2012), such as serial block-face scanning electron microscopy (SBEM) (Denk and Horstmann, 2004). A large amount of heavy metal staining is necessary for SBEM to generate sufficient back-scatter electron signal and prevent specimen charging (Deerinck et al., 2010; Kelley et al., 1973; Tapia et al., 2012). Therefore, it remains impossible to image cryofixed samples with SBEM or other techniques that require high-contrast staining.

To overcome these limitations of cryofixation, here we present a robust approach, named the CryoChem Method (CCM), which combines key advantages of cryofixation and chemical fixation. This technique enables labeling of target structures by genetically encoded EM tags or fluorescent markers in cryofixed samples, and permits high-contrast *en bloc* heavy metal staining sufficient for SBEM. Specifically, we rehydrate cryofixed samples after freeze-substitution to make the specimen suitable for subsequent aqueous reactions and fluorescence imaging. We successfully apply CCM to multiple biologically significant systems with distinct ultrastructural morphologies, including cultured mammalian cells, *Drosophila* olfactory organ (antenna) and mouse brain. By overcoming critical technical barriers, our method exploits the potential of cryofixation, making it compatible with genetically encoded EM tags and any EM techniques that require substantial heavy metal staining. Furthermore, the versatility of CCM allows us to achieve 3D CLEM in a well-preserved mouse brain by permitting SBEM after fluorescent imaging of a frozen-rehydrated specimen.

## RESULTS

Given that a key limitation of cryofixation arises from the dehydrated state of the samples after freeze-substitution (Table 1), it is imperative that our approach delivers a cryofixed specimen that is fully hydrated and can then be processed at higher temperatures (4 °C or room temperature) for enzymatic reactions and/or high-contrast *en bloc* heavy metal

staining. It has been demonstrated that cryofixed samples can be rehydrated for immunogold labeling or fluorescence imaging following cryosectioning (Dhonukshe et al., 2007; Ripper et al., 2008; Stierhof and El Kasmi, 2010; van Donselaar et al., 2007), but these approaches only yield modest EM contrast. In addition, the methods are incompatible with volume EM techniques and have yet to be successfully combined with genetic labeling using APEX2.

## **The CryoChem Method**

To achieve the ultrastructural preservation of cryofixation and the versatility of chemical fixation, we developed a hybrid protocol which we refer to hereafter as the CryoChem Method (CCM) (Table 1). Importantly, we devised a freeze-substitution cocktail (see below) that allows preservation of APEX2 enzymatic activity and signals from fluorescent proteins. CCM begins with high-pressure freezing of the sample, followed by freeze-substitution in an acetone solution with glutaraldehyde (0.2%), uranyl acetate (0.1%), methanol (2%) and water (1%), to further stabilize the cryo-preserved structures at low temperatures. After freeze-substitution, the sample is rehydrated gradually on ice with a series of acetone solutions containing an increasing amount of water or 0.1M HEPES. Once completely rehydrated, the cryofixed sample is amenable for imaging with fluorescence microscopy, DAB labeling reactions using genetically encoded tags, and the high-contrast *en bloc* staining (e.g. osmium-thiocarbohydrazide-osmium and uranyl acetate) normally reserved only for chemically fixed samples. Afterwards, samples are dehydrated through a series of ethanol solutions and acetone, then infiltrated with epoxy resin and cured using standard EM procedures. To minimize volume artefact, epoxy resin is chosen because it causes minimal tissue shrinkage during embedding (<2%) compared to other embedding media (Kushida, 1962). These resin embedded samples may be sectioned or imaged directly with any desired EM technique (Figure 1, see *Materials and Methods* for details).

## **CryoChem Method offers high-quality ultrastructural preservation and sufficient *en bloc* staining for SBEM**

To determine whether CCM provides high-quality ultrastructural preservation, we first tested the method in a mammalian cell line. Using transmission electron microscopy (TEM), well-preserved mitochondria and nuclear membranes were observed in the CCM-processed cells (Figure 2—figure supplement 1). Given that cryofixation is often necessary for properly fixing tissues surrounded by a barrier to chemical fixatives (Steinbrecht, 1980; Steinbrecht and Müller, 1987), we next tested CCM in a *Drosophila* olfactory organ, the antenna, which is encased in a waxy cuticle (Figure 2A and 2B). A hallmark of optimally preserved antennal tissues prepared by cryofixation is the smooth appearance of membrane structures (Shanbhag et al., 1999, 2000; Steinbrecht, 1980; Steinbrecht and Müller, 1987). In the insect antenna, auxiliary cells extend microlamellae to surround the olfactory receptor neurons (ORNs), forming the most membrane-rich regions in the antenna. We therefore focused on this structure to evaluate the quality of morphological preservation afforded by our method. In CCM-processed antennal tissues, we found that the delicate structures of the microlamellae were well-preserved (Figure 2B and Figure 2—video supplement 1), unlike the chemically fixed counterparts in which microlamellae were disorganized and distorted (Figure 2A) (Steinbrecht, 1980). Furthermore, there were numerous signs of extraction of cellular materials in the chemically fixed antenna (Figure 2A1, arrows), but not in the CCM-processed specimen (Figure 2B). Importantly, the overall ultrastructural preservation achieved through CCM resembles that obtained by standard cryofixation and freeze-substitution protocols (Shanbhag et al., 1999, 2000). This observation also suggests that the rehydration step in CCM leads to little, if any, swelling in the antenna tissue.

In contrast to fly antennae, which can be dissected expeditiously and frozen in the live state, certain tissues (e.g., mouse brain) are difficult to cryofix from life without tissue damage caused by anoxia or mechanical stress associated with dissection. In these cases, cryofixation

can be performed after aldehyde perfusion and still produce quality morphological preservation (Sosinsky et al., 2008). To test whether CCM can improve morphological preservation of aldehyde-perfused samples, we cryofixed vibratome sections (100  $\mu$ m) from an aldehyde-perfused mouse brain and processed the sample with CCM. Compared to specimens processed by a standard EM preparation method that involved dehydration on ice (Figure 2C), the CCM-processed samples, which were initially dehydrated through freeze-substitution, showed smoother membranes and an increase in cytoplasmic density (Figure 2D). This result indicates an improvement in morphological preservation and agrees with our previous observation that cellular morphology can be markedly improved even when cryofixation is performed after aldehyde perfusion (Sosinsky et al., 2008).

Of note, we adopted a high-contrast *en bloc* staining protocol (Deerinck et al., 2010; Tapia et al., 2012; West et al., 2010; Williams et al., 2011) when processing the *Drosophila* antennae and mouse brain. An adequate level of heavy metals was incorporated into these cryofixed samples to allow for successful imaging by SBEM (Figure 2B and 3), even without nitrogen gas injection to dissipate any charge build-up that often occurs on samples of low conductivity (Deerinck et al., 2017) (Figure 2—video supplement 1 and Figure 3D). This *en bloc* staining protocol is normally reserved only for chemically fixed tissues, but is now made compatible with cryofixed samples by CCM.

### **CryoChem Method enables DAB labeling in cryofixed samples expressing APEX2**

Next we determined if DAB labeling reaction can be performed in cryofixed samples with CCM (Figure 3A). Using CCM-processed cultured cells expressing APEX2, we observed DAB labeling in the targeted organelles (mitochondria) in the transfected cells, compared to the untransfected controls (Figure 3B). We further validated this approach in CCM-processed *Drosophila* antenna; successful DAB labeling was also detected in genetically identified ORNs expressing APEX2 with X-ray microscopy (Figure 3—video supplement 1). This imaging

technique facilitates the identification of the region of interest for SBEM (Figure 3C), as we and others reported previously (Bushong et al., 2015; Ng et al., 2016). Crucially, we demonstrated that an EM volume of a genetically labeled, cryofixed ORN can be acquired with SBEM, which allows for an accurate 3D reconstruction of the ORN through semi-automated segmentation (Figure 3D). Taken together, these results demonstrate that CCM can reliably generate DAB labeling by genetically encoded EM tags in cryofixed samples.

### **Fluorescence is well-preserved in CryoChem-processed samples**

To determine whether CCM is compatible with fluorescence microscopy, we first evaluated the degree to which fluorescence level is affected after CCM processing. Using confocal microscopy, we quantified GFP fluorescence in the soma of unfixed *Drosophila* ORNs and that from CCM-processed samples after rehydration (Figure 4). Remarkably, GFP fluorescence intensities of fresh and CCM-processed ORNs are essentially indistinguishable with respect to their distributions (Figure 4A) and average levels (Figure 4B). This result indicates that CCM processing has little effect on GFP fluorescence in fly ORNs, likely due to the use of mild fixatives during freeze-substitution in our protocol. Similarly, we observed strong GFP signals in the mouse brain after the cryofixed sample was rehydrated (Figure 4—figure supplement 1A).

Next, we asked whether this observation also applies to another type of fluorescence protein. To this end, we examined tdTomato fluorescence in the mouse brain (Figure 4—figure supplement 1B). We note that tdTomato is not a variant of GFP and is instead derived from *Discosoma sp.* fluorescence protein ‘DsRed’ (Shaner et al., 2004). Confocal images of the CCM-processed mouse brain showed that the tdTomato fluorescence was also well-preserved (Figure 4—figure supplement 1B) and we were able to detect the co-expression of GFP and tdTomato in a subpopulation of neurons (Figure 4—figure supplement 1C). Together, our results indicate that CCM-processed sample can serve as a robust substrate for fluorescence imaging.

As such, CCM allows fluorescence imaging to be combined with DAB labeling and high-contrast *en bloc* staining in the same cryofixed sample, a critical advance to cryofixation-rehydration methods (Dhonukshe et al., 2007; Ripper et al., 2008; Stierhof and El Kasmi, 2010; van Donselaar et al., 2007).

### **3D correlative light and electron microscopy (CLEM) in CCM-processed samples expressing fluorescent markers**

Finally, we took advantage of the fact that fluorescence microscopy can take place in a cryofixed sample before resin embedding to develop a protocol for 3D CLEM in CCM-processed specimens (Figure 5A, see *Materials and Methods* for details), so that the correlation can be achieved in optimally preserved tissues. The protocol first uses the core CCM steps to deliver a frozen-rehydrated sample. Subsequently, DRAQ5 DNA stain is introduced to the sample to label the nuclei, which can then serve as fiducial markers for CLEM. Next, the region containing target cells expressing fluorescent markers is imaged with confocal microscopy, during which signals from DRAQ5 and fluorescent markers are both acquired. After confocal microscopy, the sample is *en bloc* stained with multiple layers of heavy metals (Deerinck et al., 2010; Tapia et al., 2012; West et al., 2010; Williams et al., 2011), then dehydrated and embedded as in a typical CCM protocol. Subsequently, the embedded sample is imaged with X-ray microscopy. The resulting micro-computed tomography volume can be registered to the confocal volume using the nuclei as fiducial markers, so that the region of interest (ROI) for SBEM can be identified. After SBEM imaging, the EM volume can be registered to the confocal volume in a similar fashion for 3D CLEM.

As a proof of principle, we performed 3D CLEM in an aldehyde-perfused, CCM-processed mouse brain expressing tdTomato in a subset of neurons. To this end, we first determined if DRAQ5 staining can be performed in a frozen-rehydrated specimen. Using confocal microscopy, we were able to observe DRAQ5 labeling of the nuclei in a cryofixed brain



slice after rehydration (Figure 5B). We used the labeled nuclei as fiducial markers to register the X-ray volume with the confocal data (Figure 5B) and thereby target a ROI with tdTomato-expressing neurons for SBEM imaging.

Similarly, we were able to register the confocal volume to the SBEM volume (Figure 5C). Of note, the CLEM accuracy was ensured by using a subset of DRAQ5-labeled heterochromatin structures and their corresponding counterparts in EM as finer fiducial points (Figure 5C). Furthermore, the fluorescent markers made it possible to identify the target cell bodies (Figure 5D and Figure 5—video supplement 1) in the SBEM volume. The high accuracy of correlation achieved by our 3D CLEM protocol is demonstrated by the successful alignments of multiple ultrastructures: fine neuronal processes (Figure 5E) and a subcellular heterochromatin structure that was not used as a fiducial marker (Figure 5—figure supplement 1). Lastly, we note that with CCM, fluorescence microscopy in cryofixed specimens takes place before *en bloc* EM staining. Therefore, our protocol does not require special resins for embedding and permits high-contrast staining with high concentrations of osmium tetroxide.

## DISCUSSION

We described here a hybrid method, named CryoChem, which combines key advantages of cryofixation and chemical fixation to substantially broaden the applicability of the optimal fixation technique. With CCM, it is now possible to label target structures with DAB by a genetically encoded EM tag and deposit high-contrast *en bloc* staining in cryofixed tissues. In addition, with CCM, one can also image cells expressing fluorescent markers before resin embedding and perform 3D CLEM in cryofixed specimens. Our method thereby provides an alternative to conventional cryofixation and chemical fixation methods.

The modular nature of CCM (Figure 1) makes it highly versatile as researchers can modify the modules to best suit their needs. For instance, to prevent over-staining, one can replace the high-contrast *en bloc* staining step (osmium-thiocarbohydrazide-osmium and uranyl

acetate) (Deerinck et al., 2010; Tapia et al., 2012; West et al., 2010; Williams et al., 2011) with a single round of osmium tetroxide staining for thin section TEM (Figures 2C, 2D and 3B) or electron tomography. In addition, CCM is essentially compatible with a wide range of reactions catalyzed by EM tags other than APEX2 (Ellisman et al., 2015). For example, the protein labeling reactions mediated by miniSOG (Shu et al., 2011) and the tetracysteine-based methods using FIAsh and ReAsH (Gaietta et al., 2002), or the non-protein biomolecule labeling reactions using Click-EM (Ngo et al., 2016) or ChromEM (Ou et al., 2017). The versatility of CCM will likely expand the breath of biological questions that can be addressed using cryofixed samples.

In addition to using EM tags, we have also developed a 3D CLEM protocol (Figure 5A) that allows optimally preserved EM structures to be genetically labeled with fluorescent markers in CCM-processed tissues. In contrast to EM tags, fluorescent markers do not generate electron-dense products (e.g. DAB polymers) that can obscure the subcellular structures. Moreover, with multicolor CLEM, one can utilize multiple readily available genetically encoded fluorescent markers to label different target structures or cells. Using the 3D CLEM protocol, one could also pinpoint labeled subcellular structures (e.g., microtubules) or proteins (e.g., ion channels) in an EM volume with super-resolution microscopy. Furthermore, the ability to genetically label target neurons with fluorescent markers or EM tags in CCM-processed tissues can facilitate circuit reconstructions of identified neurons in optimally preserved specimens.

The advantages of CCM makes it particularly suited for addressing biological questions that require optimal and rapid preservation of a genetically labeled structure. For example, to construct an accurate model to describe the biophysical properties of a neuron, it is essential to acquire morphological measurements based on faithfully preserved ultrastructures. CCM processing provides such an opportunity; we were able to obtain a 3D reconstruction of a genetically labeled *Drosophila* ORN at nanoscale resolution with quality morphological preservation (Figure 3D). In addition, by combining CCM with Flash-and-Freeze EM (Watanabe et al., 2014) and electron tomography, it is possible to capture the fast morphological changes

of genetically labeled vesicles in 3D during synaptic transmission.

Despite its versatility, multiple factors could potentially limit the applicability of CCM. First, given that the core fixation step of CCM is cryofixation, the size of the sample is constrained by the vitrification limit of up to approximately 500  $\mu\text{m}$  (Dahl and Staehelin, 1989; McDonald, 1999; Moor, 1987; Shimon et al., 1998). In addition, freeze damage due to ice crystal formation can occur (Korogod et al., 2015; Ripper et al., 2008; Shanbhag et al., 2000). Therefore, one should be mindful of freeze damage when performing ultrastructural analysis. Moreover, CCM can only improve the temporal resolution of biological events captured if the specimen is frozen in the live state, but not when the sample was first chemically fixed (e.g. aldehyde-perfused mouse brain). Finally, there are also concerns that some molecules may be lost during rehydration if they are not properly fixed during freeze-substitution (Ripper et al., 2008).

In conclusion, CCM is applicable to addressing questions in diverse tissue types, as demonstrated here with cultured mammalian cells or tissues of *Drosophila* antennae and mouse brains. Notably, identical solutions and experimental conditions were used for these different tissues in all core steps (Figure 1). Thus, the protocol described here can likely be readily adapted to cells and tissues of other biological systems. In addition, we demonstrated that CCM can further improve the ultrastructure of an aldehyde-perfused brain (Figure 2C and 2D). Given that aldehyde perfusion is often required for the dissection of deeply embedded or fragile tissues, the compatibility of CCM with aldehyde fixation further broadens the applicability of the method.

321 **MATERIALS AND METHODS**322 **Key resources table**

Reagent type (species) or resource	Designation	Source or reference	Identifiers	Additional information
genetic reagent ( <i>Drosophila melanogaster</i> )	Or47b-GAL4	(Fishilevich and Vosshall, 2005)	RRID:BDSC_9984	
genetic reagent ( <i>D. melanogaster</i> )	Or22a-GAL4	(Dobritsa et al., 2003)	RRID:BDSC_9951	
genetic reagent ( <i>D. melanogaster</i> )	10XUAS-myc-APEX2-Orco	this study		see Materials and Methods
genetic reagent ( <i>D. melanogaster</i> )	10XUAS-mCD8GFP-APEX2	this study		see Materials and Methods
genetic reagent ( <i>Mus musculus</i> )	B6.Cg-Crhl <sup>tm1(cre)Zjh</sup> /J	Jackson Laboratory	031559 RRID:IMSR_JAX:031559	
genetic reagent ( <i>M. musculus</i> )	B6.Cg-Gt.ROSA.26Sor <sup>tm14(CAG-tdTomato)Hze</sup> /J	Jackson Laboratory	007914 RRID:IMSR_JAX:007914	
genetic reagent ( <i>M. musculus</i> )	TH-GFP	(Kessler et al., 2003)		
cell line	HEK 293T	ATCC	CRL-3216 RRID:CVCL_0063	
antibody	DRAQ5	Cell Signaling Technology	4084	1:1000
recombinant DNA reagent (plasmids)	pcDNA3-Mito-V5-APEX2	(Lam et al., 2015)	Addgene_72480	
recombinant DNA reagent (plasmids)	APEX2 DNA	(Lam et al., 2015)	Addgene_49386	
recombinant DNA reagent (plasmids)	APEX2-Orco	this study		see Materials and Methods
recombinant DNA reagent (plasmids)	mCD8GFP-APEX2	this study		see Materials and Methods
chemical compound, drug	paraformaldehyde	Fisher Scientific	04042-500	

chemical compound, drug	glutaraldehyde	Ted Pella	18426	
chemical compound, drug	sodium cacodylate	Ted Pella	18851	
chemical compound, drug	CaCl <sub>2</sub>	Sigma-Aldrich	223506	
chemical compound, drug	glycine	Bio-Rad Laboratories	161-0718	
chemical compound, drug	BSA	Sigma-Aldrich	9048-46-8	
chemical compound, drug	1-hexadecene	Sigma-Aldrich	H2131	
chemical compound, drug	uranyl acetate	Electron Microscopy Sciences	22400	
chemical compound, drug	methanol	Fisher Scientific	A412-4	
chemical compound, drug	acetone	ACROS Organics	AC326800010	
chemical compound, drug	HEPES	Gibco	15-630-080	
chemical compound, drug	diaminobenzidine; DAB	Sigma-Aldrich	D5637	
chemical compound, drug	H <sub>2</sub> O <sub>2</sub>	Fisher Scientific	H325-100	
chemical compound, drug	osmium tetroxide; OsO <sub>4</sub>	Electron Microscopy Sciences	19190	
chemical compound, drug	potassium ferrocyanide	Mallinckrodt	6932	
chemical compound, drug	thiocarbohydrazide	Electron Microscopy Sciences	21900	
chemical compound, drug	Durcupan ACM resin component A	Sigma Aldrich	44611	
chemical compound, drug	Durcupan ACM resin component B	Sigma Aldrich	44612	
chemical compound, drug	Durcupan ACM resin component C	Sigma Aldrich	44613	
chemical compound, drug	Durcupan ACM resin component D	Sigma Aldrich	44614	
chemical compound, drug	conductive silver epoxy	Ted Pella	16043	

software, algorithm	IMOD	(Kremer et al., 1996)	RRID:SCR_003297	<a href="http://bio3d.colorado.edu/imod/">http://bio3d.colorado.edu/imod/</a>
software, algorithm	ImageJ	NIH	RRID:SCR_003070	<a href="https://imagej.nih.gov/ij/">https://imagej.nih.gov/ij/</a>
software, algorithm	Amira 6.3	ThermoFisher	RRID:SCR_014305	
other	Aclar	Electron Microscopy Sciences	50426	
other	FocusClear	Cedarlane Labs	FC-101	

## **Cultured cells preparation**

HEK 293T cells (ATCC, Gaithersburg, MD) were grown on 1.2 mm diameter punches of Aclar (2 mil thick; Electron Microscopy Sciences, Hatfield, PA) for 48 hours, in a humidified cell culture incubator with 5% CO<sub>2</sub> at 37 °C. Authentication was guaranteed by ATCC, including STR profiling. The cells were negative for mycoplasma, as confirmed by using the Universal Mycoplasma Detection Kit (ATCC, Gaithersburg, MD). The culture medium used was DMEM (Mediatech Inc., Manassas, VA) supplemented with 10% fetal bovine serum (Gemini Bio-Products, West Sacramento, CA). The cells were transfected with Lipofectamine 2000 (Invitrogen, Carlsbad, CA) with a plasmid carrying APEX2 targeted to mitochondria (pcDNA3-Mito-V5-APEX2, Addgene #72480; Lam et al., 2015). At 24 hours after transfection, the cells were used for CCM processing.

## **DNA constructs and *Drosophila* transgenesis**

Orco cDNA was a gift from Dr. Aidan Kiely, and APEX2 DNA was acquired from Addgene (APEX2-NES, #49386). Membrane targeting of APEX2 was achieved by fusing the marker protein to the C-terminus of mCD8GFP or to the N-terminus of Orco. Briefly, gel-purified PCR fragments of mCD8GFP, APEX2, and/or Orco were pieced together with Gibson Assembly following manufacturer's instructions (New England Biolabs, Ipswich, MA). A linker (SGGGG) was added between APEX2 and its respective fusion partner. In the APEX2-Orco construct, a myc tag was included in the primer and added to the N-terminus of APEX2 to enable the detection of the fusion protein by immunostaining. To facilitate Gateway Cloning (ThermoFisher Scientific, Waltham, MA), the attB1 and attB2 sites were included in the primers and added to the ends of the Gibson assembly product by PCR amplification. The PCR products were then

purified and cloned into pDONR221 vectors via BP Clonase II (Life Technologies, Carlsbad, CA). The entry clones were recombined into the pBID-UASC-G destination vector (Wang et al., 2012) using LR Clonases II (Life Technologies, Carlsbad, CA).

*Drosophila* transgenic lines were derived from germline transformations using the  $\Phi$ C31 integration systems (Groth et al., 2004; Markstein et al., 2008). All transgenes described in this study were inserted into the attP40 landing site on the second chromosome (BestGene Inc., Chino Hills, CA). Target expression of APEX2 and mCD8GFP in the ORNs was driven by the Or47b-GAL4 driver (#9984, Bloomington *Drosophila* Stock Center; Fishilevich & Vosshall, 2005; Figures 2-4) or the Or22a-GAL4 driver (#9951, Bloomington *Drosophila* Stock Center; Dobritsa et al. 2003, Figure 3—video supplement 1). Flies were raised on standard cornmeal food at 25°C in a 12:12 light-dark cycle.

### ***Drosophila* antennae preparation**

Six to eight days old flies were cold anesthetized and then pinned to a Sylgard dish. The third segments of the antennae were removed from the head of the fly with a pair of fine forceps and then immediately transferred to a drop of 1X PBS on the dish. With a sharp glass microelectrode, a hole was poked in the antenna to facilitate solution exchange. It is critical that the tissue remained in PBS at all times to prevent deflation. The antenna should remain plump and maintain its shape prior to cryofixation.

### **Chemical fixation of *Drosophila* antenna**



Antennae were dissected as described above, and then incubated at 4 °C for 18 hours in Karnovsky fixatives: 2% paraformaldehyde (Fisher Scientific, Hampton, NH)/2.5% glutaraldehyde (Ted Pella, Redding, CA)/2 mM  $\text{CaCl}_2$  (Sigma-Aldrich, St. Louis, MO) in 0.1 M sodium cacodylate (Ted Pella, Redding, CA). Next, samples were washed in 0.1 M sodium cacodylate for 10 minutes and in a solution of 100 mM glycine (Bio-Rad Laboratories, Hercules, CA) in 0.1 M sodium cacodylate for another 10 minutes, and twice more in 0.1 M sodium cacodylate. All washing steps were performed on ice. The following *en bloc* heavy metal staining, dehydration and resin embedding steps were carried out as described in the CryoChem Method section below.

## **Transgenic mice and virus-mediated gene transfer**

Animals were handled in accordance with the guidelines established by the *Guide for Care and Use of Laboratory Animals* and approved by UCSD Animal Care and Use Committee. To introduce GFP and tdTomato fluorescent markers in a mouse brain (Figure 4—figure supplement 1), GFP was expressed in the tyrosine hydroxylase (TH)-expressing neurons and tdTomato in the corticotropin releasing factor (CRF)-expressing neurons. A CRF driver mouse line (B6.Cg-Crh<sup>tm1(cre)Zjh</sup>/J, Jackson laboratory) expressing CRE recombinase under the control of the Crh promoter/enhancer elements was first crossed to a tdTomato reporter line (B6.Cg-Gt.ROSA.26Sor<sup>tm14(CAG-tdTomato)Hze</sup>/J, Jackson Laboratory). The progeny was then crossed to a TH-GFP mouse line (Kessler et al., 2003), obtaining a transgenic model stably expressing GFP in dopaminergic (TH<sup>+</sup>) neurons and CRE/tdTomato in CRF-releasing neurons. To test the 3D CLEM protocol and the morphological preservation offered by CCM (Figure 2C, 2D and 5, Figure 5—figure supplement 1 and Figure 5—video supplement 1), a mouse brain from a

tdTomato reporter line (B6.Cg-Gt.ROSA.26Sor<sup>tm14(CAG-tdTomato)Hze</sup>/J, Jackson Laboratory) was used.

## Mouse brain preparation

Mice were anesthetized with ketamine/xylazine and then transcardially perfused with Ringer's solution followed by 0.15 M sodium cacodylate containing 4% paraformaldehyde/0.2% (Figure 4—figure supplement 1) or 0.5% (Figure 2C, 2D and 5, Figure 5—figure supplement 1 and Figure 5—video supplement 1) glutaraldehyde/2 mM CaCl<sub>2</sub>. The animal was perfused for 10 minutes with the fixatives and then the brain was removed and placed in ice-cold fixative for 1 hour. The brain was then cut into 100-µm thick slices using a vibrating microtome. Slices were either processed for chemical fixation (Figure 2C) or stored in ice-cold 0.15 M sodium cacodylate for around 4 hours until used for high-pressure freezing (Figure 2D, Figure 4—figure supplement 1, Figure 5, Figure 5—figure supplement 1 and Figure 5—video supplement 1).

## Chemical fixation of mouse brain

The aldehyde-perfused mouse brain slices were post-fixed in 2.5% glutaraldehyde for 20 minutes, then washed with 0.15 M sodium cacodylate five times for 5 minutes on ice. Next, the samples were incubated in 0.15 M sodium cacodylate with 100 mM glycine for 5 minutes on ice, then washed in 0.15 M sodium cacodylate similarly. The following *en bloc* heavy metal staining, dehydration and resin embedding steps were carried out as described in the CryoChem Method section below.

## **CryoChem Method:**

### **(I) Cryofixation by high-pressure freezing**

*Cultured cells:* Aclar disks were placed within the well of a 100  $\mu\text{m}$ -deep membrane carrier. The cells were covered with the culture medium and then high-pressure frozen with a Leica EM Pact 2 unit.

*Drosophila antennae:* The third antennal segment was dissected as described above. Antennae from the same fly were transferred into the 100  $\mu\text{m}$ -deep well of a type A planchette filled with 20% BSA (Sigma-Aldrich, St. Louis, MO) in 0.15 M sodium cacodylate. The well of the type A planchette was then covered with the flat side of a type B planchette to secure the sample. The samples were immediately loaded into a freezing holder and frozen with a high-pressure freezing machine (Bal-Tec HPM 010). Planchettes used for cryofixation were pre-coated with 1-hexadecene (Sigma-Aldrich, St. Louis, MO) to prevent planchettes A and B from adhering to each other so as to allow solution to reach the samples during freeze-substitution.

*Mouse brain slices:* A 1.2 mm tissue puncher was used to cut a portion of hypothalamus expressing tdTomato (Figure 2D, Figure 4—figure supplement 1, Figure 5, Figure 5—figure supplement 1 and Figure 5—video supplement 1) and GFP (Figure 4—figure supplement 1) from a tissue slice. The tissue punch was placed into a 100  $\mu\text{m}$ -deep membrane carrier and surrounded with 20% BSA in 0.15 M sodium cacodylate. The specimen was high-pressure frozen as described for the *Drosophila antennae*.

All frozen samples were stored in liquid nitrogen until further processing.

### **(II) Freeze-substitution**

Frozen samples in planchettes were transferred in a liquid nitrogen bath to cryo-vials containing the freeze-substitution solution. To prepare the freeze-substitution solution of 0.2%

glutaraldehyde, 0.1% uranyl acetate, 2% methanol and 1% water in acetone, a 10 mL solution was prepared by adding 80  $\mu$ L of 25% aqueous glutaraldehyde, 200  $\mu$ L of 5% uranyl acetate (Electron Microscopy Sciences, Hatfield, PA) dissolved in methanol, and 20  $\mu$ L of water to acetone (ACROS Organics, USA). Next, the sample vials were transferred to a freeze-substitution device (Leica EM AFS2) at -90 °C for 58 hours, from -90 °C to -60 °C for 15 hours (with the temperature raised at 2 °C/hr), at -60 °C for 15 hours, from -60 °C to -30 °C for 15 hours (at +2 °C/hr), and then at -30 °C for 15 hours. In the last hour at -30°C, samples were washed three times in an acetone solution with 0.2% glutaraldehyde and 1% water for 20 minutes. The cryo-tubes containing the last wash were then transferred on ice for an hour.

### **(III) Rehydration**

The freeze-substituted samples were then rehydrated gradually in a series of nine rehydration solutions (see below). The samples were transferred from the freeze-substitution solution to the first rehydration solution (5% water, 0.2% glutaraldehyde in acetone) on ice for 10 minutes. The rehydration step was repeated in a stepwise manner until the samples were fully rehydrated in the final rehydration solution (0.1 M and 0.15 M sodium cacodylate for cells and antennae or mouse brain slices, respectively) (van Donselaar et al., 2007):

- 1) 5% water, 0.2% glutaraldehyde in acetone
- 2) 10% water, 0.2% glutaraldehyde in acetone
- 3) 20% water, 0.2% glutaraldehyde in acetone
- 4) 30% water, 0.2% glutaraldehyde in acetone
- 5) 50% 0.1M HEPES (Gibco, Taiwan), 0.2% glutaraldehyde in acetone
- 6) 70%, 0.1M HEPES, 0.2% glutaraldehyde in acetone
- 7) 0.1 M HEPES

459 8) 0.1 M / 0.15 M sodium cacodylate with 100 mM glycine

460 9) 0.1 M / 0.15 M sodium cacodylate

461 After rehydration, samples were removed from the planchettes using a pair of forceps  
462 under a stereo microscope to a 0.1 M (cells and antenna) / 0.15 M (brain) sodium cacodylate  
463 solution in a scintillation vial on ice. It is important that subsequent DAB labeling and *en bloc*  
464 heavy metal staining are carried out in scintillation vials instead of the planchettes because  
465 metal planchettes may react with the labeling or staining reagents.

#### 466 **(IV) DRAQ5 staining**

467 Mouse brain slices were incubated in DRAQ5 (1:1000 in 0.15 M sodium cacodylate  
468 buffer; Cell Signaling Technology, Danvers, MA) on ice for 60 minutes. Then the samples were  
469 washed in 0.15 M sodium cacodylate three times for 10 minutes on ice before fluorescence  
470 imaging.

#### 471 **(V) Fluorescence imaging**

472 *Drosophila antenna*: Freshly dissected or cryofixed-rehydrated antennae (10x UAS-  
473 *mCD8GFP-APEX2*; *Or47b-GAL4*) were mounted in FocusClear (Cedarlane Labs, Burlington,  
474 Canada) between two cover glasses (#1.5 thickness, 22 mm x 22 mm, Fisher Scientific,  
475 Hampton, NH) separated by two layers of spacer rings. Confocal images were collected on an  
476 Olympus FluoView 1000 confocal microscope with a 60X water-immersion objective lens. The  
477 488 nm laser was used to excite GFP and all images were acquired at the same laser power  
478 and gain to enable comparison between the fresh vs cryofixed-rehydrated samples.

479 *Mouse brain slices*: After freeze-substitution and rehydration, the specimens were  
480 placed in ice-cold 0.15 M sodium cacodylate for imaging. Confocal images of GFP and

tdTomato signals (Figure 4—figure supplement 1) were collected on a Leica SPE II confocal microscope with a 20X water-immersion objective lens using 488 nm and 561 nm excitation. Confocal volumes of DRAQ5 and tdTomato signals (Figure 5, Figure 5—figure supplement 1, Figure 5—video supplement 1) were collected on an Olympus FluoView 1000 confocal microscope with a 20X air and 60X water objectives using 561 nm and 633 nm excitation.

## **(VI) DAB labeling of target structures by APEX2**

*Cultured cells:* Samples were transferred to a 0.05% DAB (Sigma-Aldrich, St. Louis, MO) solution in 0.1 M sodium cacodylate for 5 minutes on ice to allow DAB to diffuse into the tissue. To label the mitochondria in the APEX2-expressing cells, samples were then transferred to a 0.05% DAB solution with 0.015% H<sub>2</sub>O<sub>2</sub> (Fisher Scientific, Hampton, NH) in 0.1 M sodium cacodylate until DAB labeling was visible under a microscope (~5 minutes on ice). After the reaction, samples were washed three times with 0.1 M sodium cacodylate on ice for 10 minutes.

*Drosophila antennae:* Samples were first placed into a 0.05% DAB solution in 0.1 M sodium cacodylate for an hour on ice to allow DAB to access target neurons underneath the cuticle in the antenna. To label APEX2-expressing ORNs, antennae were then transferred into a 0.05% DAB solution with 0.015% H<sub>2</sub>O<sub>2</sub> in 0.1 M sodium cacodylate for an hour on ice. After the reaction, samples were washed three times with 0.1 M sodium cacodylate on ice for 10 minutes.

## **(VII) *en bloc* heavy metal staining for TEM and SBEM**

For TEM: Cultured cells and mouse brain slices were incubated in 2% OsO<sub>4</sub> (Electron Microscopy Sciences, Hatfield, PA)/1.5% potassium ferrocyanide (Mallinckrodt, Staines-Upon-Thames, UK )/2 mM CaCl<sub>2</sub> in 0.1 M (cells) or 0.15 M (brain) sodium cacodylate for an hour on ice. Then samples were washed in water five times for 5 minutes on ice prior to the dehydration step detailed below.

For SBEM: *Drosophila* antennae and mouse brain slices were incubated in 2% OsO<sub>4</sub>/1.5% potassium ferrocyanide/2 mM CaCl<sub>2</sub> in 0.1 M (antennae) or 0.15 M (brain) sodium cacodylate for an hour at room temperature. Then samples were washed in water five times for 5 minutes and transferred to 0.5% thiocarbohydrazide (filtered with 0.22 µm filter before use; Electron Microscopy Sciences, Hatfield, PA) for 30 minutes at room temperature. Samples were washed in water similarly and incubated in 2% OsO<sub>4</sub> for 30 minutes at room temperature. Afterwards, samples were rinsed with water, then transferred to 2% aqueous uranyl acetate (filtered with 0.22 µm filter) at 4 °C overnight. In the next morning, samples were first washed in water five times for 5 minutes and then subjected to the dehydration steps detailed below.

#### **(VIII) Dehydration**

Samples were dehydrated with a series of ethanol solutions and acetone in six steps of 10 minutes each: 70% ethanol, 90% ethanol, 100% ethanol, 100% ethanol, 100% acetone, 100% acetone. All ethanol dehydration steps were carried out on ice, and the acetone steps at room temperature. The first acetone dehydration step was carried out with ice-cold acetone, and the second one was with acetone kept at room temperature.

#### **(IX) Resin infiltration**

*Cultured cells:* Samples were transferred to a Durcupan ACM resin/acetone (1:1) solution for an hour on a shaker at room temperature. The samples were then transferred to fresh 100% Durcupan ACM resin overnight and subsequently placed in fresh resin for four hours. While in 100% resin, samples were placed in a vacuum chamber on a rocker to facilitate the removal of residual acetone. Finally, the samples were embedded in fresh resin at 60 °C for two days.

*Drosophila antennae and mouse brain slices:* Samples were transferred to a Durcupan ACM resin/acetone (1:1) solution overnight on a shaker. The next day, samples were transferred into fresh 100% Durcupan ACM resin twice, with six to seven hours apart. While in 100% resin, samples were placed in a vacuum chamber on a rocker to facilitate the removal of residual acetone. After the overnight incubation in 100% resin, samples were embedded in fresh resin at 60 °C for at least two days.

Durcupan ACM resin (Sigma Aldrich, St. Louis, MO) composition was 11.4 g component A, 10 g component B, 0.3 g component C, and 0.1 g component D.

#### **X-ray Microscopy (microcomputed tomography)**

*Drosophila antenna:* Microcomputed tomography (microCT) was performed on resin-embedded specimens using a Versa 510 X-ray microscope (Zeiss). Flat-embedded specimens were glued to the end of an aluminum rod using cyanoacrylic glue. Imaging was performed with a 40X objective using a tube current of 40 kV and no source filter. Raw data consisted of 1601 projection images collected as the specimen was rotated 360 degrees. The voxel dimension of the final tomographic reconstruction was 0.4123 µm.

*Mouse brain slices:* X-ray microscopy scan was collected of a resin-embedded sample at 80 kVp with a voxel size of 0.664 µm prior to mounting for SBEM imaging. A second scan was collected of the mounted specimen at 80 kVp with 0.7894 µm voxels.

#### **Transmission Electron Microscopy**



Ultrathin sections (70 nm) were collected on 300 mesh copper grids. Samples were post-stained with either Sato's lead solution only (cultured cells) or with 2% uranyl acetate and Sato's lead solution (mouse brain slices). Sections were imaged on an FEI Spirit TEM at 80 kV equipped with a 2k x 2k Tietz CCD camera.

## **Serial Block-face Scanning Electron Microscopy**

*Drosophila antenna*: Following microcomputed tomography to confirm proper orientation of region of interest, specimens were mounted on aluminum pins with conductive silver epoxy (Ted Pella, Redding, CA). The specimens were trimmed to remove excess resin above ROI and to remove silver epoxy from sides of specimen. The specimens were sputter coated with gold-palladium and then imaged using a Gemini scanning electron microscope (Zeiss) equipped with a 3View2XP and OnPoint backscatter detector (Gatan). Images were acquired at 2.5 kV accelerating voltage with a 30 µm condenser aperture and 1 µsec dwell time; Z step size was 50 nm; raster size was 12k x 9k and Z dimension was 1200 sections. Volumes were either collected in variable pressure mode with a chamber pressure of 30 Pa and a pixel size of 3.8 nm (Figure 2—video supplement 1 and Figure 3D) or using local gas injection (Deerinck et al., 2017) set to 85% and a pixel size of 6.5 nm (Figures 2A, 2B and 3C). Volumes were aligned using cross correlation, segmented, and visualized using IMOD (Kremer et al., 1996).

*Mouse brain slices*: SBEM was performed on a Merlin scanning electron microscope (Zeiss) equipped with a 3View2XP and OnPoint backscatter detector (Gatan). The volume was collected at 2 kV, with 6.8 nm pixels and 70 nm Z steps. Local gas injection (Deerinck et al., 2017) was set to 15% during imaging. The raster size was 10k x 15k and the Z dimension was 659 sections.

570

## 571 **Semi-automated segmentation of DAB-labeled *Drosophila* olfactory receptor neuron**

572         The DAB-labeled *Drosophila* ORN was segmented in a semi-automated fashion using  
573 the IMOD software to generate the 3D model. The IMOD command line 'imodauto' was used for  
574 the auto-segmentation by setting thresholds to isolate the labeled cellular structures of interest.  
575 Further information about the utilities of 'imodauto' can be found in the IMOD manual  
576 (<http://bio3d.colorado.edu/imod/doc/man/imodauto.html>). Auto-segmentation was followed by  
577 manual proofreading and reconstruction by two independent proofreaders. The proofreaders  
578 used elementary operations in IMOD, most commonly the 'drawing tools' to correct the contours  
579 generated by 'imodauto'. Where 'imodauto' failed to be applied successfully, the proofreaders  
580 also used the 'drawing tools' to directly trace the outline of the labeled structure. The contours of  
581 ORNs generally do not vary markedly between adjacent sections. Therefore, alternate sections  
582 were traced for the reconstruction of some parts of the ORN dendrite.

583

## 584 **Quantification of fluorescence intensity**

585         To quantify GFP fluorescence intensity shown in Figure 4, maximum intensity Z-  
586 projections were generated using ImageJ (NIH). Average fluorescence intensity in the  
587 background was subtracted from the fluorescence intensity of each cell body measured. Only  
588 non-overlapping cell bodies were quantified. Kolmogorov-Smirnov Test was performed on  
589 <http://www.physics.csbsju.edu/stats/KS-test.html> and Mann-Whitney *U* Test was performed  
590 using SigmaPlot 13.0 (Systat Software, San Jose, CA).

591

## **Light and electron microscope volume registration**

To target tdTomato-expressing cells in the mouse brain for SBEM imaging, the confocal volumes collected in the frozen-rehydrated specimen was registered with the microCT volume of the resin-embedded sample, using a software tool developed in our lab. The resin-embedded specimen was then mounted and trimmed for SBEM based on the microCT volume. A second microCT scan of the mounted specimen allowed for precise targeting of the cells of interest with the Gatan stage for SBEM. After the SBEM volume was collected, the confocal and SBEM volumes were registered using the landmark tool of Amira 6.3 (ThermoFisher, Waltham, MA). Heterochromatin structures revealed by DRAQ5 labeling and visible in the SBEM volume were used as landmark points for the registration.

**TABLE AND FIGURE LEGENDS**

**Table 1. Comparison of the advantages and limitations of different sample preparation**

**methods for electron microscopy.** The CryoChem Method (CCM) combines the advantages of chemical fixation and cryofixation. With CCM, samples are fixed with high-pressure freezing and freeze-substitution to achieve quality ultrastructural preservation. This approach allows preservation of tissues with cuticle or cell wall and captures biological events with high temporal resolution. A rehydration step is introduced to enable fluorescence imaging, DAB labeling by genetically encoded EM tags and high-contrast *en bloc* heavy metal staining of the cryofixed sample. The high-contrast *en bloc* heavy metal staining permitted by CCM reduces the need for post-staining on sections, and makes CCM compatible with serial block-face scanning electron microscopy (SBEM). Common limitations of chemical fixation and cryofixation are denoted in red.

**Figure 1. Flowchart of the CryoChem Method.** After cryofixation by high-pressure freezing and freeze-substitution, cryofixed samples are rehydrated gradually. Rehydrated samples can then be imaged for fluorescence, subjected to DAB labeling reaction or *en bloc* stained with a substantial amount of heavy metals. The protocol is modular; the first three processes are the core steps of CCM and the starred steps are optional depending on the experimental design. The samples are then dehydrated for resin infiltration and embedding, followed by imaging with any EM technique of choice. Blue and grey denote hydrated and dehydrated states of the sample, respectively.

**Figure 2. CryoChem Method offers high-quality ultrastructural preservation and sufficient**

**en bloc staining for SBEM.** EM images were acquired to assess the morphology of CCM-

processed tissues. (A-B) The quality of preservation was markedly improved in the CCM-

processed *Drosophila* antenna compared to the chemically fixed counterpart. Pixel resolution of

SBEM images (x,y): 6.5 nm. (A1 and B1) Unlike the CCM-processed antenna, the chemically

fixed antenna showed signs of extraction (arrow) and disorganized membranes. ORN: olfactory

receptor neuron; ML: microlamella (ML). Scale bar: 1  $\mu$ m. (A2 and B2) The microlamellae were

well-preserved in CCM-processed antenna, compared to chemically fixed samples. Scale bars:

1  $\mu$ m. (A3 and B3) In the enlarged views of the boxed regions, the microlamellae in the CCM-

processed antenna appeared uniform in size and shape, unlike the chemically fixed ones which

were distorted. Scale bars: 200 nm. (C-D) CCM enhanced the morphological preservation of

aldehyde-perfused mouse brain. The initial dehydration in standard EM preparation took place

on ice for 1 hour, but it occurred during freeze-substitution at -90 °C to -30 °C for over 5 days in

CCM processing. (C1 and D1) The smoothness of membranes was improved by CCM

processing. ST: synaptic terminal. Scale bar: 200 nm. Pixel resolution of TEM images (x,y): 1.92

nm. (C2 and D2) The preservation of nuclear envelopes was improved by CCM processing. N:

nucleus. Scale bar: 500 nm. Pixel resolution (x,y): 2.88 nm. (C3 and D3) In the enlarged views

of the boxed regions, the nuclear envelopes (NE; arrows) appeared smoother and the

cytoplasmic density (asterisk) was increased with CCM processing. We note that the chromatin

was more heavily stained in the CCM-processed specimen, likely due to the additional exposure

to uranyl acetate during freeze-substitution. Scale bar: 100 nm. Pixel resolution (x,y): 1.14 nm.

**Figure supplement 1 for Figure 2.** TEM images showed well-preserved ultrastructures in the

CCM-processed HEK 293T cells. In the enlarged view of the boxed region (bottom panel),

smooth nuclear membranes were observed. Scale bars: 1  $\mu$ m for the top panel, 500 nm for the

bottom panel. Pixel resolution (x,y): 6.01 nm.

**Video supplement 1 for Figure 2.** A SBEM volume from a CryoChem-processed *Drosophila* antenna. Scale bar: 500 nm. SBEM imaging parameters (only a small region of the SBEM volume acquired is shown in the video): Z step: 50 nm; Z dimension: 1200 sections; raster size: 12k x 9k; pixel size: 3.8 nm.

**Figure 3. CryoChem Method enables DAB labeling by APEX2 in cryofixed tissues.** In CCM-processed cultured cells and *Drosophila* antennae, DAB labeling was observed in cells expressing APEX2. (A) Flowchart for DAB labeling of target structures expressing APEX2 in CCM-processed samples. In our experiments, the cultured cells were imaged with TEM and the *Drosophila* antennae were imaged with X-ray microscopy, followed by SBEM. (B) Mitochondria in HEK 293T cell transfected with Mito-APEX2 were labeled with DAB (bottom panel), in contrast to an untransfected control cell (top panel). Scale bars: 200 nm. Pixel resolution (x,y): 3.97 nm (top panel); 2.88 nm (bottom panel). (C) An APEX2-expressing olfactory receptor neuron (ORN) was labeled with DAB (arrow) in the *Drosophila* antenna (*10x UAS-myc-APEX2-Orco; Or47b-GAL4*). Asterisks denote ORNs without APEX2 expression. Scale bar: 500 nm. Pixel resolution of SBEM images (x,y): 6.5 nm. (D) A series of SBEM images showing the same DAB labeled *Drosophila* ORN (arrow) in different planes of section. Asterisks denote ORNs without APEX2 expression. The images were acquired using standard imaging methods without charge compensation by nitrogen gas injection (Deerinck et al., 2017). These images, together with the rest of the EM volume acquired using SBEM, enabled semi-automatic segmentation and 3D reconstruction of the labeled ORN (right panel). Scale bars: 500 nm for SBEM images, 2  $\mu$ m for the 3D model of ORN. SBEM imaging parameters: Z step: 50 nm; Z dimension: 1200 sections; raster size: 12k x 9k; pixel size: 3.8 nm.

**Video supplement 1 for Figure 3.** An X-ray micro-computed tomography volume from a CCM-processed *Drosophila* antenna showing DAB labeling in subsets of ORNs expressing APEX2

(10x UAS-mCD8GFP-APEX2; Or22a-GAL4). The damaged region on the opposite side of the labeled cells indicates the hole poked in the antenna to facilitate solution exchange. Scale bar: 30  $\mu$ m.

**Figure 4. GFP fluorescence is well-preserved in CryoChem-processed samples.** Confocal images were taken to quantify the level of GFP fluorescence in *Drosophila* ORNs. Antennae were collected from transgenic flies expressing GFP in a subset of ORNs. (A) GFP fluorescence intensity distributions of the ORN soma in freshly-dissected, unfixed antennae (left panel) and CCM-processed antennae (right panel) are not significantly different.  $p=0.810$ , Kolmogorov-Smirnov test. Insets show representative images, with ORN soma outlined. Scale bar: 2  $\mu$ m. (B) Comparison of the average fluorescence intensities. GFP intensities are virtually identical between neurons in unfixed antennae and frozen-rehydrated antennae.  $n= 3$  antennae, Error bars denote SEM,  $p=0.950$ , Mann-Whitney  $U$  Test.

**Figure supplement 1 for Figure 4. GFP and tdTomato fluorescence in a cryofixed-rehydrated mouse brain.** (A) GFP- and (B) tdTomato-positive neurons (C) Co-expression of GFP and tdTomato fluorescence was detected in the cryofixed-rehydrated mouse brain. Scale bar: 50  $\mu$ m.

**Figure 5. 3D correlated light and electron microscopy (CLEM) in CCM-processed mouse brain.** Mouse brain slices with fluorescently labeled neurons were processed with CCM, imaged with confocal microscopy, X-ray microscopy and SBEM for 3D CLEM. (A) Flowchart for performing 3D CLEM with CCM-processed samples. Similar to a typical CCM protocol, cryofixed samples are first freeze-substituted and rehydrated. The frozen-rehydrated sample is then stained with DRAQ5 to label DNA in the nuclei. Next, the region of interest (ROI) is

identified using confocal microscopy based on fluorescent signals, while the DRAQ5 signals are also acquired to serve as fiducial markers. Subsequently, the sample is stained, dehydrated and embedded for X-ray microscopy and SBEM. Using the DRAQ5 signals as fiducial markers, the confocal volumes can be registered to the X-ray volume such that the ROI for SBEM can be identified. Once the SBEM volume is acquired, it can be registered to the confocal volumes based on the positions of the nuclei for 3D CLEM. (B) An example of the DRAQ5 fluorescence signals (left), the corresponding ROI in X-ray volume (middle) and overlay (right). This image registration process facilitates ROI identification in SBEM. Scale bar: 20  $\mu\text{m}$ . (C) DRAQ5 fluorescence labeling served as fiducial points for registering the confocal volume to the SBEM volume. Scale bar: 5  $\mu\text{m}$ . (D) The cell body of a tdTomato-expressing neuron (left) was identified in the SBEM volume (middle) through CLEM (right). (E) Neuronal processes expressing tdTomato (left) were also identified in the SBEM volume (middle) through CLEM (right). Scale bars: 2  $\mu\text{m}$ , for both (D) and (E). SBEM imaging parameters: Z step: 70 nm; Z dimension: 695 sections; raster size: 10k x 15k; pixel size: 6.8 nm.

**Figure supplement 1 for Figure 5. A Correlation of subcellular structure can be achieved using 3D CLEM performed on CCM-processed mouse brain.** A heterochromatin structure (arrow) labeled by DRAQ5 in fluorescence microscopy was identified in the SBEM volume through CLEM. This heterochromatin structure was not used as a fiducial marker for image registration. Scale bar: 1  $\mu\text{m}$ .

**Video supplement 1 for Figure 5.** A volume showing 3D CLEM in a CCM-processed mouse brain. tdTomato-expressing neurons were clearly identified in the SBEM volume. Scale bar: 10  $\mu\text{m}$ .



## REFERENCES

- Briggman, K. L., & Bock, D. D. (2012). Volume electron microscopy for neuronal circuit reconstruction. *Current Opinion in Neurobiology*, 22(1), 154–161.  
<http://doi.org/10.1016/j.conb.2011.10.022>
- Brown, E., Mantell, J., Carter, D., Tilly, G., & Verkade, P. (2009). Studying intracellular transport using high-pressure freezing and correlative light electron microscopy. *Seminars in Cell and Developmental Biology*, 20(8), 910–919. <http://doi.org/10.1016/j.semcdb.2009.07.006>
- Bushong, E. A., Johnson, D. D., Kim, K.-Y., Terada, M., Hatori, M., Peltier, S. T., Panda, S., Merkle, A., Ellisman, M. H. (2015). X-Ray microscopy as an approach to increasing accuracy and efficiency of serial block-face imaging for correlated light and electron microscopy of biological specimens. *Microscopy and Microanalysis*, 21(1), 231–238.  
<http://doi.org/10.1017/S1431927614013579>
- Dahl, R., & Staehelin, L. A. (1989). High-pressure freezing for the preservation of biological structure: Theory and practice. *Journal of Electron Microscopy Technique*, 13(3), 165–174.  
<http://doi.org/10.1002/jemt.1060130305>
- de Boer, P., Hoogenboom, J. P., & Giepmans, B. N. G. (2015). Correlated light and electron microscopy: Ultrastructure lights up! *Nature Methods*, 12(6), 503–513.  
<http://doi.org/10.1038/nmeth.3400>
- Deerinck, T., Bushong, E., Lev-Ram, V., Shu, X., Tsien, R., & Ellisman, M. (2010). Enhancing serial block-face scanning electron microscopy to enable high resolution 3-D nanohistology of cells and tissues. *Microscopy and Microanalysis*, 16(S2), 1138–1139.  
<http://doi.org/10.1017/S1431927610055170>
- Deerinck, T. J., Shone, T. M., Bushong, E. A., Ramachandra, R., Peltier, S. T., & Ellisman, M. H. (2017). High-performance serial block-face SEM of nonconductive biological samples

744 enabled by focal gas injection-based charge compensation. *Journal of Microscopy*, 0(0), 1–  
745 8. <http://doi.org/10.1111/jmi.12667>

746 Denk, W., & Horstmann, H. (2004). Serial block-face scanning electron microscopy to  
747 reconstruct three-dimensional tissue nanostructure. *PLoS Biology*, 2(11), e329.  
748 <http://doi.org/10.1371/journal.pbio.0020329>

749 Dhonukshe, P., Aniento, F., Hwang, I., Robinson, D. G., Mravec, J., Stierhof, Y. D., & Friml, J.  
750 (2007). Clathrin-mediated constitutive endocytosis of PIN auxin efflux carriers in  
751 Arabidopsis. *Current Biology*, 17(6), 520–527. <http://doi.org/10.1016/j.cub.2007.01.052>

752 Ding, R. (1993). Three-dimensional reconstruction and analysis of mitotic spindles from the  
753 yeast, *Schizosaccharomyces pombe*. *The Journal of Cell Biology*, 120(1), 141–151.  
754 <http://doi.org/10.1083/jcb.120.1.141>

755 Dobritsa, A. A, van der Goes van Naters, W., Warr, C. G., Steinbrecht, R. A., & Carlson, J. R.  
756 (2003). Integrating the molecular and cellular basis of odor coding in the *Drosophila*  
757 antenna. *Neuron*, 37(5), 827–41. <http://www.ncbi.nlm.nih.gov/pubmed/12628173>

758 Doroquez, D. B., Berciu, C., Anderson, J. R., Sengupta, P., & Nicastro, D. (2014). A high-  
759 resolution morphological and ultrastructural map of anterior sensory cilia and glia in  
760 *Caenorhabditis elegans*. *eLife*, 2014(3), 1–35. <http://doi.org/10.7554/eLife.01948>

761 Ellisman, M. H., Deerinck, T. J., Kim, K. Y., Bushong, E. A., Phan, S., Ting, A. Y., & Boassa, D.  
762 Advances in molecular probe-based labeling tools and their application to multiscale  
763 multimodal correlated microscopies. *Journal of Chemical Biology*.  
764 <http://doi.org/10.1007/s12154-015-0132-6>

765 Fishilevich, E., & Vosshall, L. B. (2005). Genetic and functional subdivision of the *Drosophila*  
766 antennal lobe. *Current Biology: CB*, 15(17), 1548–53.

767 <http://doi.org/10.1016/j.cub.2005.07.066>

768 Gaietta, G., Deerinck, T. J., Adams, S. R., Bouwer, J., Tour, O., Laird, D. W., Sosinsky, G. E.,  
 769 Tsien, R. Y., Ellisman, M. H. (2002). Multicolor and electron microscopic imaging of  
 770 connexin trafficking. *Science*, 296(5567), 503–507. <http://doi.org/10.1126/science.1068793>

771 Groth, A. C., Fish, M., Nusse, R., & Calos, M. P. (2004). Construction of transgenic *Drosophila*  
 772 by using the site-specific integrase from phage  $\Phi$ C31. *Genetics*, 166(4), 1775–1782.  
 773 <http://doi.org/10.1534/genetics.166.4.1775>

774 Hess, M. W., Müller, M., Debbage, P. L., Vetterlein, M., & Pavelka, M. (2000). Cryopreparation  
 775 provides new insight into the effects of brefeldin A on the structure of the HepG2 Golgi  
 776 apparatus. *Journal of Structural Biology*, 130(1), 63–72.  
 777 <http://doi.org/10.1006/jsbi.2000.4230>

778 Joesch, M., Mankus, D., Yamagata, M., Shahbazi, A., Schalek, R., Suissa-Peleg, A., Meister,  
 779 M., Lichtman, J. W., Scheirer, W. J., Sanes, J. R. (2016). Reconstruction of genetically  
 780 identified neurons imaged by serial-section electron microscopy. *eLife*, 5(e15015), 1-13.  
 781 <http://doi.org/10.7554/eLife.15015>

782 Kaeser, W., Koyro, H. -W, & Moor, H. (1989). Cryofixation of plant tissues without pretreatment.  
 783 *Journal of Microscopy*, 154(3), 279–288. <http://doi.org/10.1111/j.1365-2818.1989.tb00591.x>

784 Kellenberger, E., Johansen, R., Maeder, M., Bohrmann, B., Stauffer, E., & Villiger, W. (1992).  
 785 Artefacts and morphological changes during chemical fixation. *Journal of Microscopy*,  
 786 168(2), 181–201. <http://doi.org/10.1111/j.1365-2818.1992.tb03260.x>

787 Kelley, R. O., Dekker, R. A. F., & Bluemink, J. G. (1973). Ligand-mediated osmium binding: Its  
 788 application in coating biological specimens for scanning electron microscopy. *Journal of*  
 789 *Ultrastructure Research*, 45(3–4), 254–258. [http://doi.org/10.1016/S0022-5320\(73\)80051-6](http://doi.org/10.1016/S0022-5320(73)80051-6)

790 Kessler, M. A, Yang, M., Gollomp, K. L., Jin, H., & Iacovitti, L. (2003). The human tyrosine

791 hydroxylase gene promoter. *Molecular Brain Research*, 112(1–2), 8–23.  
 792 [http://doi.org/10.1016/S0169-328X\(02\)00694-0](http://doi.org/10.1016/S0169-328X(02)00694-0)

793 Kiss, J. Z., Giddings, T. H., Staehelin, L. A., & Sack, F. D. (1990). Comparison of the  
 794 ultrastructure of conventionally fixed and high pressure frozen/freeze substituted root tips  
 795 of *Nicotiana* and *Arabidopsis*. *Protoplasma*, 157(1–3), 64–74.  
 796 <http://doi.org/10.1007/BF01322639>

797 Kolotuev, I., Schwab, Y., & Labouesse, M. (2010). A precise and rapid mapping protocol for  
 798 correlative light and electron microscopy of small invertebrate organisms. *Biology of the*  
 799 *Cell*, 102(2), 121–132. <http://doi.org/10.1042/BC20090096>

800 Korogod, N., Petersen, C. C. H., & Knott, G. W. (2015). Ultrastructural analysis of adult mouse  
 801 neocortex comparing aldehyde perfusion with cryo fixation. *eLife*, 4(e05793), 1–17.  
 802 <http://doi.org/10.7554/eLife.05793>

803 Kremer, J. R., Mastronarde, D. N., & McIntosh, J. R. (1996). Computer visualization of three-  
 804 dimensional image data using IMOD. *Journal of Structural Biology*, 116(1), 71–76.  
 805 <http://doi.org/10.1006/jsbi.1996.0013>

806 Kukulski, W., Schorb, M., Welsch, S., Picco, A., Kaksonen, M., & Briggs, J. A. G. (2011).  
 807 Correlated fluorescence and 3D electron microscopy with high sensitivity and spatial  
 808 precision. *Journal of Cell Biology*, 192(1), 111–119. <http://doi.org/10.1083/jcb.201009037>

809 Kushida, H. (1962). A study of cellular swelling and shrinkage during fixation, dehydration and  
 810 embedding in various standard media. *Journal of Electron Microscopy*, 11(3), 135–138.  
 811 <http://doi.org/10.1093/oxfordjournals.jmicro.a049346>

812 Lam, S. S., Martell, J. D., Kamer, K. J., Deerinck, T. J., Ellisman, M. H., Mootha, V. K., & Ting,  
 813 A. Y. (2015). Directed evolution of APEX2 for electron microscopy and proximity labeling.  
 814 *Nature Methods*, 12(1), 51–54. <http://doi.org/10.1038/nmeth.3179>

815 Leapman, R. D. (2004). Novel techniques in electron microscopy. *Current Opinion in*  
816 *Neurobiology*, 14(5), 591–598. <http://doi.org/10.1016/j.conb.2004.08.004>

817 Markstein, M., Pitsouli, C., Villalta, C., Celniker, S. E., & Perrimon, N. (2008). Exploiting position  
818 effects and the gypsy retrovirus insulator to engineer precisely expressed transgenes.  
819 *Nature Genetics*, 40(4), 476–483. <http://doi.org/10.1038/ng.101>

820 Martell, J. D., Deerinck, T. J., Sancak, Y., Poulos, T. L., Mootha, V. K., Sosinsky, G. E., ... Ting,  
821 A. Y. (2012). Engineered ascorbate peroxidase as a genetically encoded reporter for  
822 electron microscopy. *Nature Biotechnology*, 30(11), 1143–8.  
823 <http://doi.org/10.1038/nbt.2375>

824 McDonald, K. (1999). High-pressure freezing for preservation of high resolution fine structure  
825 and antigenicity for immunolabeling. In *Electron Microscopy Methods and Protocols* (Vol.  
826 117, pp. 77–98). New Jersey: Humana Press. <http://doi.org/10.1385/1-59259-201-5:77>

827 McDonald, K. (2007). Cryopreparation methods for electron microscopy of selected model  
828 systems. *Methods in Cell Biology*. [http://doi.org/10.1016/S0091-679X\(06\)79002-1](http://doi.org/10.1016/S0091-679X(06)79002-1)

829 McDonald, K. (2009). A review of high-pressure freezing preparation techniques for correlative  
830 light and electron microscopy of the same cells and tissues. *Journal of Microscopy*, 235(3),  
831 273–281. <http://doi.org/10.1111/j.1365-2818.2009.03218.x>

832 Moor, H. (1987). Theory and practice of high pressure freezing. In R. A. Steinbrecht & K. Zierold  
833 (Eds.), *Cryotechniques in Biological Electron Microscopy* (pp. 175–191). Berlin, Heidelberg:  
834 Springer Berlin Heidelberg. [http://doi.org/10.1007/978-3-642-72815-0\\_8](http://doi.org/10.1007/978-3-642-72815-0_8)

835 Müller-Reichert, T., Hohenberg, H., O'Toole, E. T., & McDonald, K. (2003). Cryoimmobilization  
836 and three-dimensional visualization of *C. elegans* ultrastructure. *Journal of Microscopy*,  
837 212(1), 71–80. <http://doi.org/10.1046/j.1365-2818.2003.01250.x>

838 Ng, J., Browning, A., Lechner, L., Terada, M., Howard, G., Jefferis, G. S. X. E. (2016).

839 Genetically targeted 3D visualisation of *Drosophila* neurons under electron microscopy and  
840 X-Ray microscopy using miniSOG. *Scientific Reports*, 6(1), 38863.  
841 <http://doi.org/10.1038/srep38863>

842 Ngo, J. T., Adams, S. R., Deerinck, T. J., Boassa, D., Rodriguez-Rivera, F., Palida, S. F.,  
843 Carolyn, R. B., Ellisman, M. H., Tsien, R. Y. (2016). Click-EM for imaging metabolically  
844 tagged nonprotein biomolecules. *Nature Chemical Biology*, 12(6), 459–465.  
845 <http://doi.org/10.1038/nchembio.2076>

846 Nixon, S. J., Webb, R. I., Floetenmeyer, M., Schieber, N., Lo, H. P., Parton, R. G. (2009). A  
847 single method for cryofixation and correlative light, electron microscopy and tomography of  
848 zebrafish embryos. *Traffic*, 10(2), 131–136. [http://doi.org/10.1111/j.1600-](http://doi.org/10.1111/j.1600-0854.2008.00859.x)  
849 [0854.2008.00859.x](http://doi.org/10.1111/j.1600-0854.2008.00859.x)

850 Ou, H. D., Phan, S., Deerinck, T. J., Thor, A., Ellisman, M. H., O'Shea, C. C. (2017).  
851 ChromEMT: Visualizing 3D chromatin structure and compaction in interphase and mitotic  
852 cells. *Science*, 357(6349), eaag0025. <http://doi.org/10.1126/science.aag0025>

853 Ripper, D., Schwarz, H., & Stierhof, Y.-D. (2008). Cryo-section immunolabelling of difficult to  
854 preserve specimens: advantages of cryofixation, freeze-substitution and rehydration.  
855 *Biology of the Cell*, 100(2), 109–123. <http://doi.org/10.1042/BC20070106>

856 Ryan, K., Lu, Z., Meinertzhagen, I. A. (2016). The CNS connectome of a tadpole larva of *Ciona*  
857 intestinalis (L.) highlights sidedness in the brain of a chordate sibling. *eLife*, 5(e16962), 1–  
858 34. <http://doi.org/10.7554/eLife.16962>

859 Sabatini, D. D. (1963). Cytochemistry and electron microscopy: The preservation of cellular  
860 ultrastructure and enzymatic activity by aldehyde fixation. *The Journal of Cell Biology*,  
861 17(1), 19–58. <http://doi.org/10.1083/jcb.17.1.19>

862 Schwarz, H., Humbel, B. (2009). Correlative light and electron microscopy. In A. Cavalier, D.

863 Spehner, B. Humbel (Eds.), *Handbook of cryo-preparation methods for electron*  
864 *microscopy*. (pp. 537–565). CRC Press.

865 Shanbhag, S. R., Müller, B., Steinbrecht, R. A. (1999). Atlas of olfactory organs of *Drosophila*  
866 *melanogaster* 1. Types, external organization, innervation and distribution of olfactory  
867 sensilla. *International Journal of Insect Morphology and Embryology*, 28(4), 377–397.  
868 [http://doi.org/10.1016/S0020-7322\(99\)00039-2](http://doi.org/10.1016/S0020-7322(99)00039-2)

869 Shanbhag, S. R., Müller, B., Steinbrecht, R. A. (2000). Atlas of olfactory organs of *Drosophila*  
870 *melanogaster* 2. Internal organization and cellular architecture of olfactory sensilla.  
871 *Arthropod Structure & Development*, 29(3), 211–229. [http://doi.org/10.1016/S1467-](http://doi.org/10.1016/S1467-8039(00)00028-1)  
872 [8039\(00\)00028-1](http://doi.org/10.1016/S1467-8039(00)00028-1)

873 Shaner, N. C., Campbell, R. E., Steinbach, P. A., Giepmans, B. N. G., Palmer, A. E., Tsien, R.  
874 Y. (2004). Improved monomeric red, orange and yellow fluorescent proteins derived from  
875 *Discosoma* sp. red fluorescent protein. *Nature Biotechnology*, 22(12), 1567–1572.  
876 <http://doi.org/10.1038/nbt1037>

877 Shimoni, E., Müller, M., Mueller, M. (1998). On optimizing high-pressure freezing: from heat  
878 transfer theory to a new microbioopsy device. *Journal of Microscopy*, 192(Pt 3), 236–247.  
879 Retrieved from <http://www.ncbi.nlm.nih.gov/pubmed/9923416>

880 Shu, X., Lev-Ram, V., Deerinck, T. J., Qi, Y., Ramko, E. B., Davidson, M. W., Jin, Y., Ellisman,  
881 M. H., Tsien, R. Y. (2011). A genetically encoded tag for correlated light and electron  
882 microscopy of intact cells, tissues, and organisms. *PLoS Biology*, 9(4), e1001041.  
883 <http://doi.org/10.1371/journal.pbio.1001041>

884 Sosinsky, G. E., Crum, J., Jones, Y. Z., Lanman, J., Smarr, B., Terada, M., Martone, M. E.,  
885 Deerinck, T. J., Johnson, J. E., Ellisman, M. H. (2008). The combination of chemical  
886 fixation procedures with high pressure freezing and freeze substitution preserves highly

887 labile tissue ultrastructure for electron tomography applications. *Journal of Structural*  
888 *Biology*, 161(3), 359–371. <http://doi.org/10.1016/j.jsb.2007.09.002>

889 Steinbrecht, R. A. (1980). Cryofixation without cryoprotectants. Freeze substitution and freeze  
890 etching of an insect olfactory receptor. *Tissue and Cell*, 12(1), 73–100.  
891 [http://doi.org/10.1016/0040-8166\(80\)90053-1](http://doi.org/10.1016/0040-8166(80)90053-1)

892 Steinbrecht, R. A., Müller, M. (1987). Freeze-substitution and freeze-drying. In R. A. Steinbrecht  
893 & K. Zierold (Eds.), *Cryotechniques in Biological Electron Microscopy* (pp. 149–172).  
894 Berlin, Heidelberg: Springer Berlin Heidelberg. [http://doi.org/10.1007/978-3-642-72815-0\\_7](http://doi.org/10.1007/978-3-642-72815-0_7)

895 Stierhof, Y. D., & El Kasmi, F. (2010). Strategies to improve the antigenicity, ultrastructure  
896 preservation and visibility of trafficking compartments in Arabidopsis tissue. *European*  
897 *Journal of Cell Biology*, 89(2–3), 285–297. <http://doi.org/10.1016/j.ejcb.2009.12.003>

898 Szczesny, P. J., Walther, P., Müller, M. (1996). Light damage in rod outer segments: The effects  
899 of fixation on ultrastructural alterations. *Current Eye Research*, 15(8), 807–814.  
900 <http://doi.org/10.3109/02713689609017621>

901 Takemura, S., Bharioke, A., Lu, Z., Nern, A., Vitaladevuni, S., Rivlin, P. K., ... Chklovskii, D. B.  
902 (2013). A visual motion detection circuit suggested by Drosophila connectomics. *Nature*,  
903 500(7461), 175–181. <http://doi.org/10.1038/nature12450>

904 Tapia, J. C., Kasthuri, N., Hayworth, K. J., Schalek, R., Lichtman, J. W., Smith, S. J., Buchanan,  
905 J. (2012). High-contrast en bloc staining of neuronal tissue for field emission scanning  
906 electron microscopy. *Nature Protocols*, 7(2), 193–206.  
907 <http://doi.org/10.1038/nprot.2011.439>

908 van Donselaar, E., Posthuma, G., Zeuschner, D., Humbel, B. M., Slot, J. W. (2007).  
909 Immunogold labeling of cryosections from high-pressure frozen cells. *Traffic*, 8(5), 471–  
910 485. <http://doi.org/10.1111/j.1600-0854.2007.00552.x>



911 Wang, J.-W., Beck, E. S., & McCabe, B. D. (2012). A modular toolset for recombination  
 912 transgenesis and neurogenetic analysis of *Drosophila*. *PLoS One*, 7(7), e42102.  
 913 <https://doi.org/10.1371/journal.pone.0042102>

914 Watanabe, S., Davis, M. W., & Jorgensen, E. M. (2014). Flash-and-freeze electron microscopy:  
 915 coupling optogenetics with high-pressure freezing. In U. V. Nägerl & A. Triller (Eds.),  
 916 *Nanoscale Imaging of Synapses. Neuromethods* (pp. 43–57). New York, NY: Humana  
 917 Press. [http://doi.org/10.1007/978-1-4614-9179-8\\_3](http://doi.org/10.1007/978-1-4614-9179-8_3)

918 Watanabe, S., Liu, Q., Davis, M. W., Hollopeter, G., Thomas, N., Jorgensen, N. B., Jorgensen,  
 919 E. M. (2013). Ultrafast endocytosis at *Caenorhabditis elegans* neuromuscular junctions.  
 920 *eLife*, 2013(2), 1–24. <http://doi.org/10.7554/eLife.00723>

921 Watanabe, S., Punge, A., Hollopeter, G., Willig, K. I., Hobson, R. J., Davis, M. W., Hell, S. W.,  
 922 Jorgensen, E. M. (2011). Protein localization in electron micrographs using fluorescence  
 923 nanoscopy. *Nature Methods*, 8(1), 80–84. <http://doi.org/10.1038/nmeth.1537>

924 Watanabe, S., Rost, B. R., Camacho-Pérez, M., Davis, M. W., Söhl-Kielczynski, B.,  
 925 Rosenmund, C., Jorgensen, E. M. (2013). Ultrafast endocytosis at mouse hippocampal  
 926 synapses. *Nature*, 504(7479), 242–247. <http://doi.org/10.1038/nature12809>

927 Watanabe, S., Trimbuch, T., Camacho-Pérez, M., Rost, B. R., Brokowski, B., Söhl-Kielczynski,  
 928 B., Felies, A., Davis, M. W., Rosenmund, C., Jorgensen, E. M. (2014). Clathrin regenerates  
 929 synaptic vesicles from endosomes. *Nature*, 515(7526), 228–233.  
 930 <http://doi.org/10.1038/nature13846>

931 West, J. B., Fu, Z., Deerinck, T. J., Mackey, M. R., Obayashi, J. T., Ellisman, M. H. (2010).  
 932 Structure-function studies of blood and air capillaries in chicken lung using 3D electron  
 933 microscopy. *Respiratory Physiology and Neurobiology*, 170(2), 202–209.  
 934 <http://doi.org/10.1016/j.resp.2009.12.010>

935 Williams, M. E., Wilke, S. A., Daggett, A., Davis, E., Otto, S., Ravi, D., Ripley, B., Bushong, E.  
936 A., Ellisman, M. H., Klein, G., Ghosh, A. (2011). Cadherin-9 regulates synapse-specific  
937 differentiation in the developing hippocampus. *Neuron*, 71(4), 640–655.  
938 <http://doi.org/10.1016/j.neuron.2011.06.019>

939 Winey, M., Mamay, C. L., O'Toole, E. T., Mastronarde, D. N., Giddings, T. H., McDonald, K. L.,  
940 McIntosh, J. R. (1995). Three-dimensional ultrastructural analysis of the *Saccharomyces*  
941 *cerevisiae* mitotic spindle. *Journal of Cell Biology*, 129(6), 1601–1615.  
942 <http://doi.org/10.1083/jcb.129.6.1601>

943 Zheng, Z., Lauritzen, J. S., Perlman, E., Robinson, C. G., Nichols, M., Milkie, D., ... Bock, D. D.  
944 (2017). A complete electron microscopy volume of the brain of adult *Drosophila*  
945 *melanogaster*. *bioRxiv*. <http://doi.org/doi.org/10.1101/140905>

946

## ACKNOWLEDGEMENTS

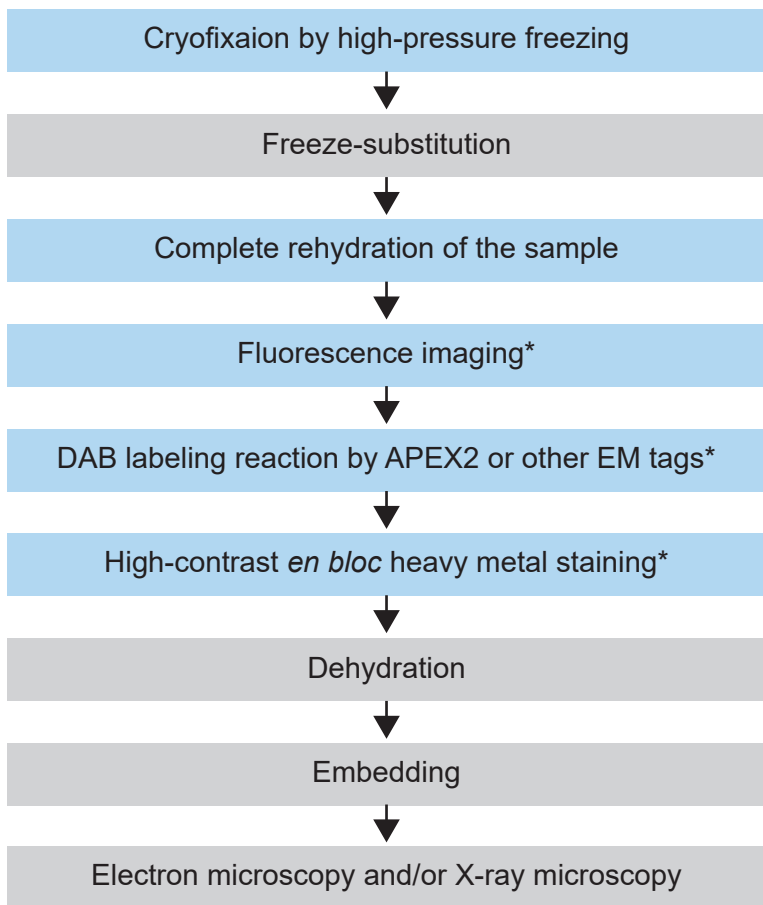
We thank Aiden Keily for providing the Orco cDNA construct and R. Alexander Steinbrecht for advice on electron microscopy of *Drosophila* antennae. We also thank Edie Zhang and Martin Orden for assistance in segmentation of *Drosophila* olfactory receptor neuron. We also thank Andrea Thor and Mason Mackey for help with EM sample preparation and imaging. We also thank Steven Wasserman for comments on the manuscript. This work was supported by Frontiers of Innovation Scholars Program and Croucher Foundation Scholarship to TKT, the Ray Thomas Edwards Foundation Career Development Award, Kavli Institute for Brain and Mind Innovative Research Grant (2015-004) and NIH R01DC015519 to CYS. This work was also supported by a grant to MHE P41GM103412 from the National Institute of General Medical Sciences for support of the National Center for Microscopy and Imaging Research (NCMIR) technologies and instrumentation, the NIH R01GM086197 to DB and Kavli Institute for Brain and Mind Innovative Research Grant (2016-038) to DB & DD. The authors declare no conflicts of interest.

962 Table 1

	Chemical fixation	Cryofixation	CryoChem
Fixation	Aldehyde fixatives (4 °C)	1) High-pressure freezing (-196 °C, ~2100 bar)  2) Freeze-substitution in organic solvents	1) High-pressure freezing (-196 °C, ~2100 bar)  2) Freeze-substitution in organic solvents
Ultrastructural preservation	Fair	Excellent	Excellent
Tissues with cuticle or cell wall	Incompatible	Compatible	Compatible
Temporal resolution of events captured	Low	High	High
Hydration state of the sample	Hydrated	Dehydrated after freeze-substitution	Hydrated after rehydration
Fluorescence imaging after fixation	Compatible	Generally incompatible	Compatible
DAB labeling by genetic EM tags	Compatible	Incompatible due to dehydration	Compatible due to rehydration
High-contrast <i>en bloc</i> heavy metal staining	Compatible	Limited	Compatible due to rehydration
Post-staining on sections	Optional	Often required	Optional
SBEM compatibility	Compatible	Incompatible	Compatible

963

Figure 1



Sample hydrated

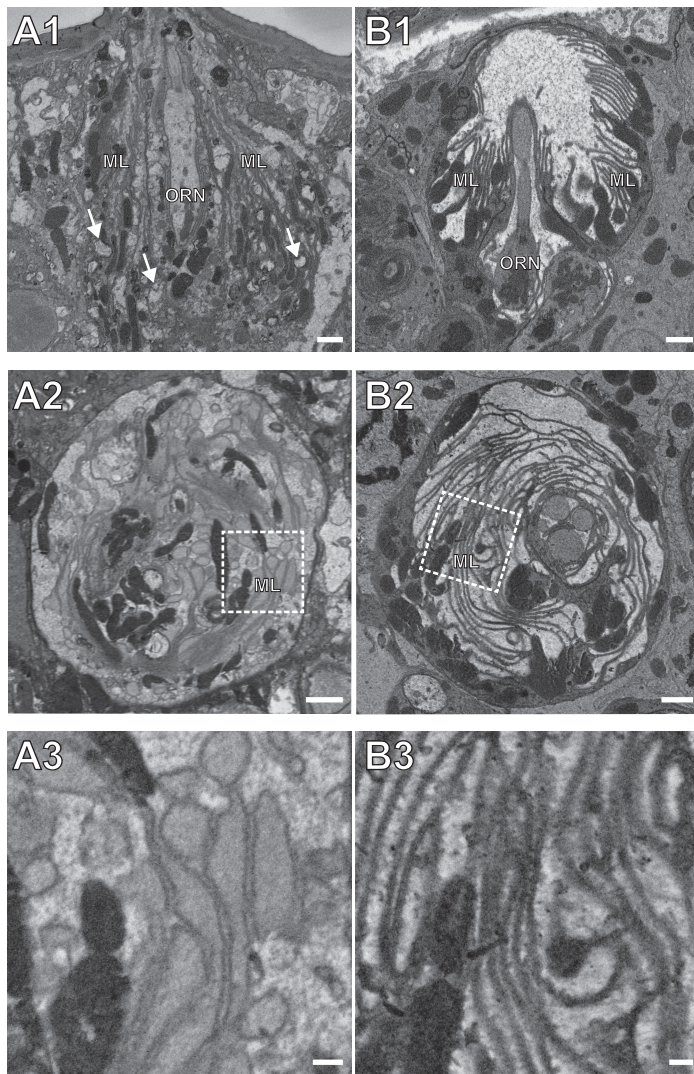
Sample dehydrated

Figure 2

*Drosophila* antenna (SBEM)

Chemical fixation

CryoChem



Aldehyde-perfused mouse brain (TEM)

Standard EM preparation  
(dehydration: 4°C)

CryoChem  
(dehydration: -90°C to -30°C)

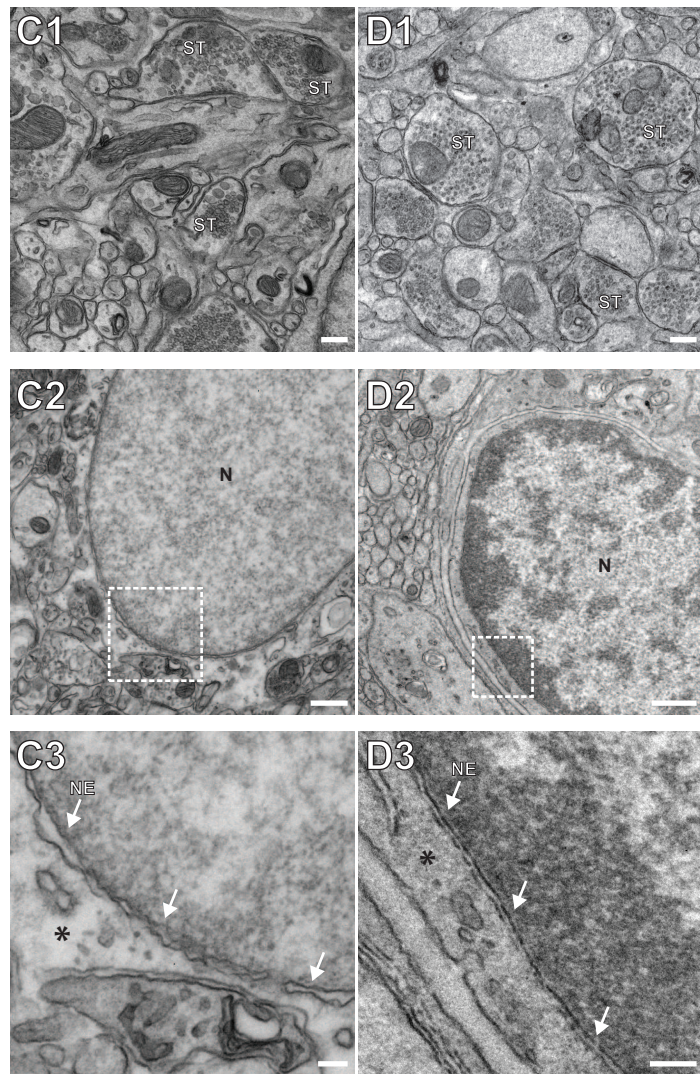




# Figure 2-figure supplement 1

Cultured mammalian cells (TEM)

CryoChem

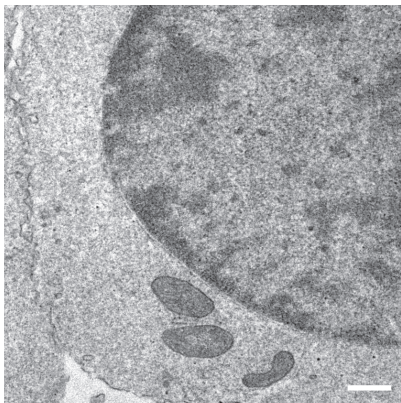
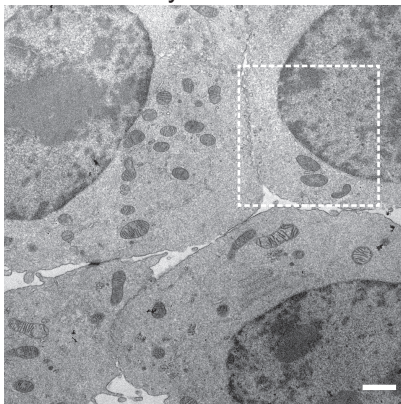


Figure 3

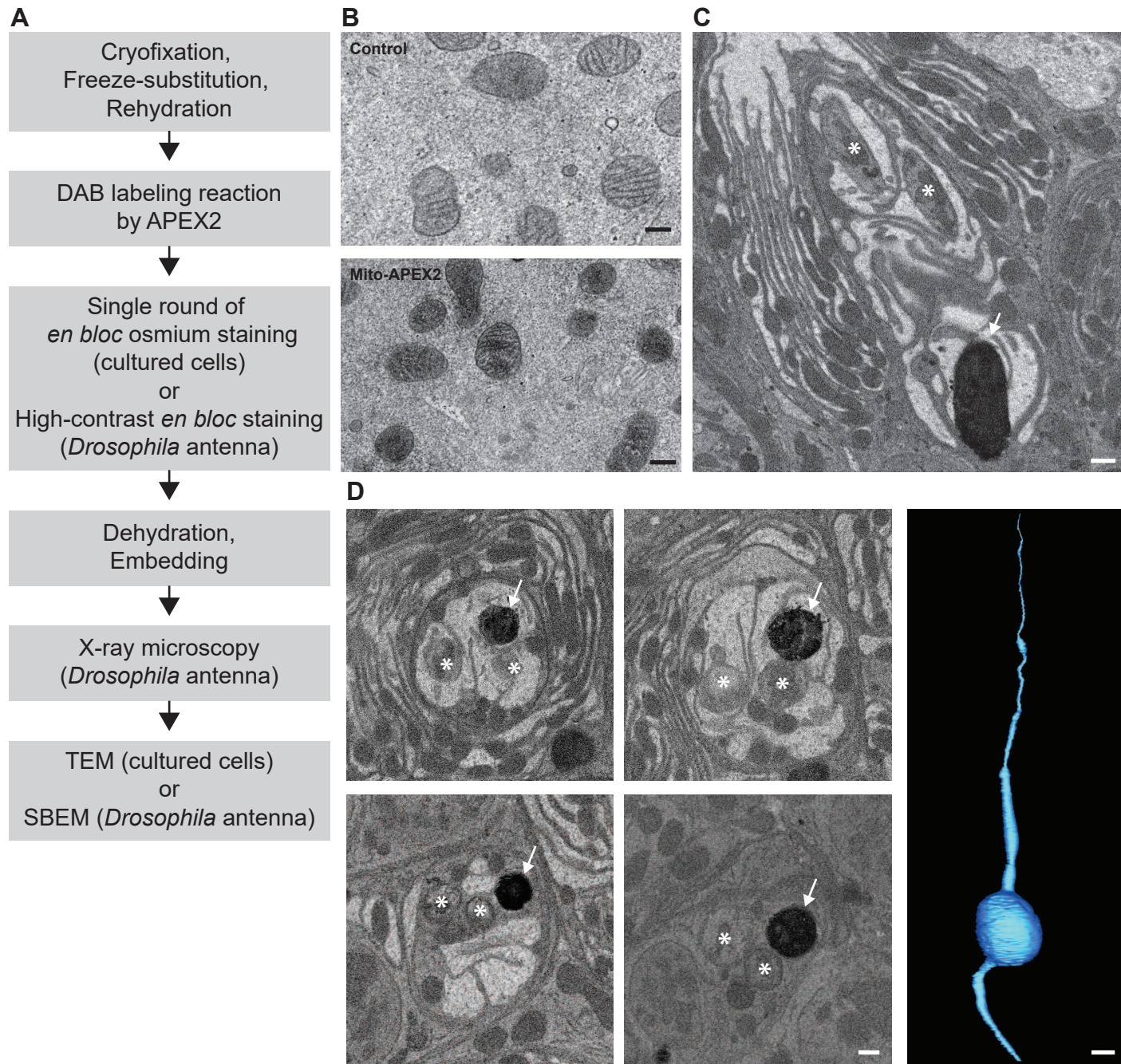




Figure 4

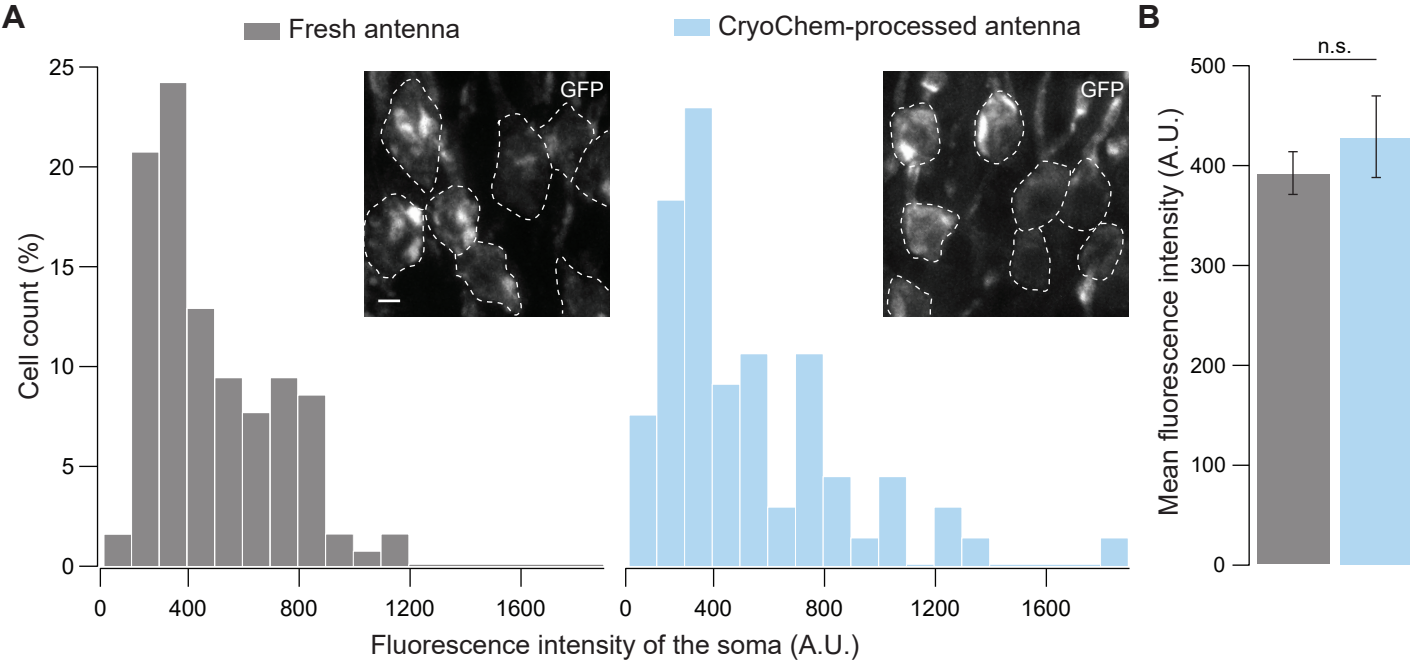


Figure 4-figure supplement 1

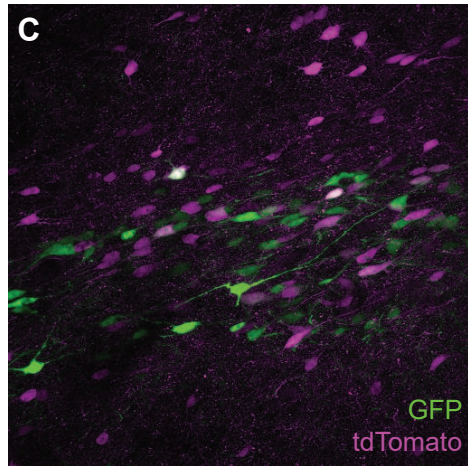
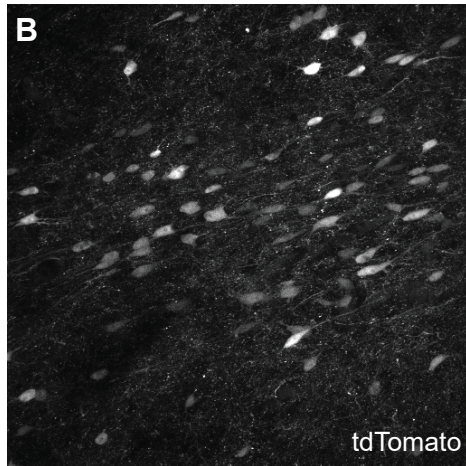
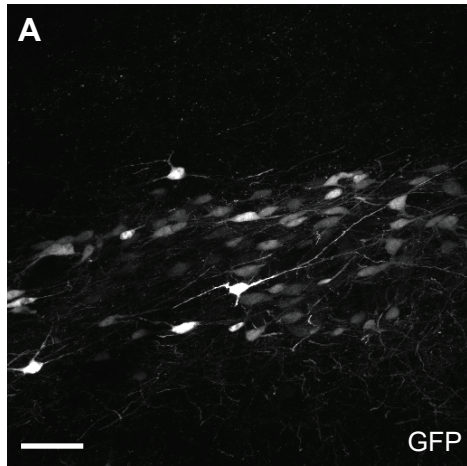
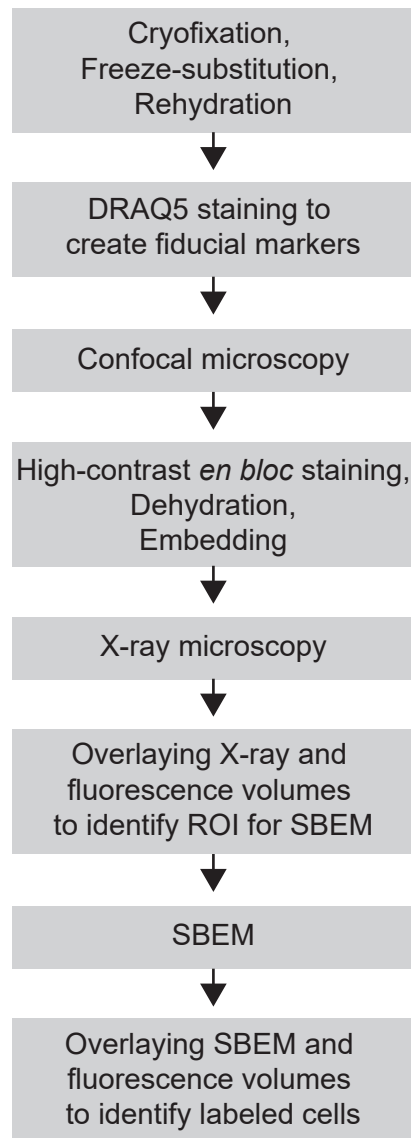
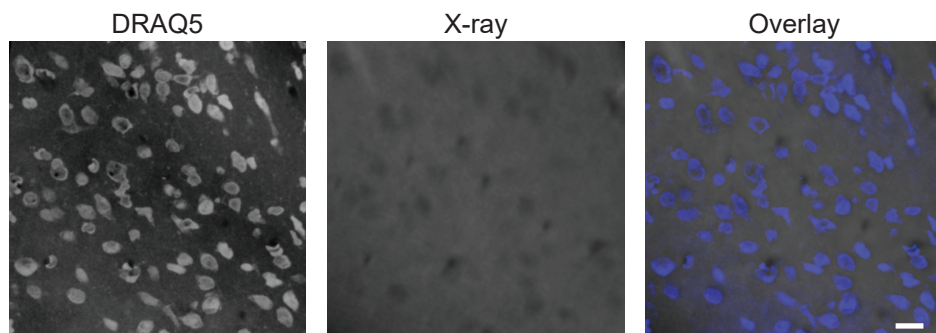


Figure 5

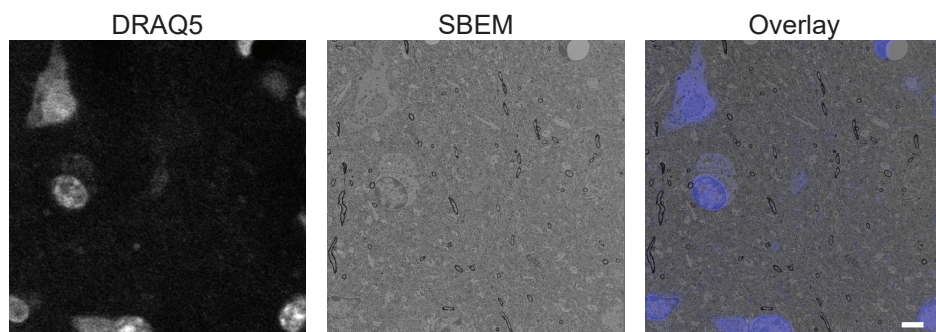
**A**



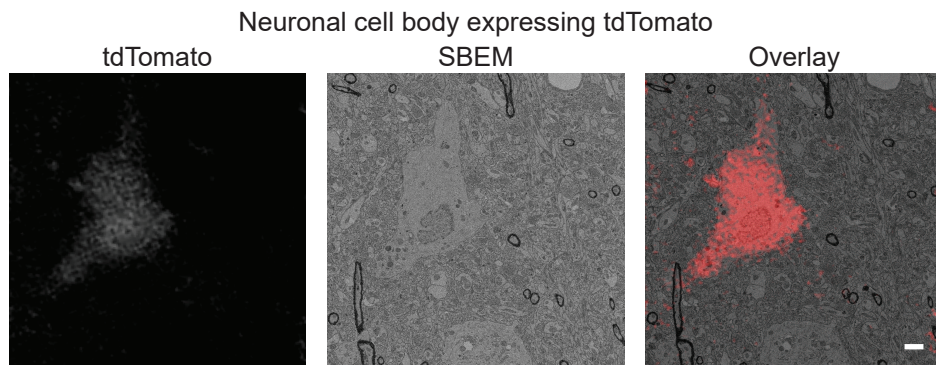
**B**



**C**



**D**



**E**

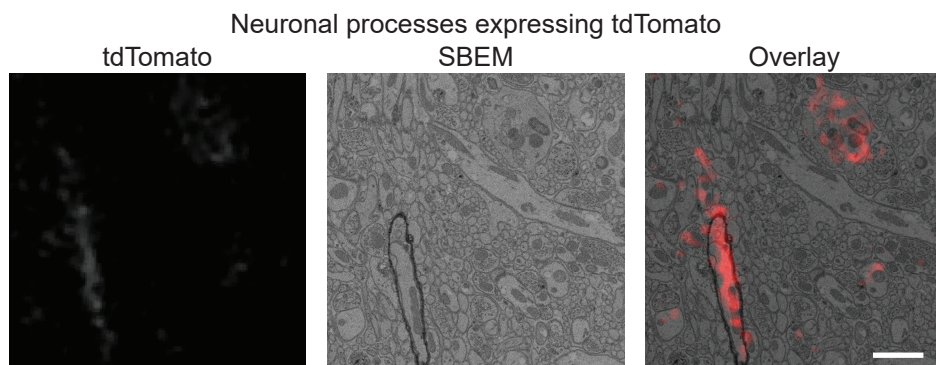
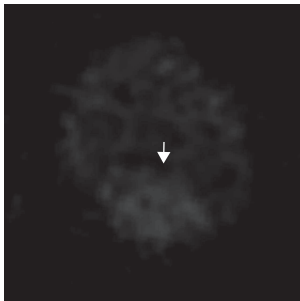
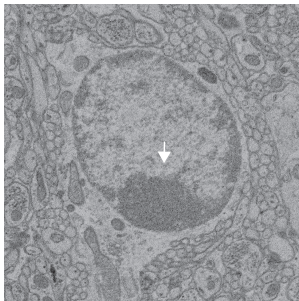


Figure 5-figure supplement 1

DRAQ5



SBEM



Overlay

